A study on radio-resistance mechanism of cancer stem-like cells using a property of low proteasome activity in canine tumor cell lines

(犬腫細胞株におけるプロテアソーム活性を用いて分離したがん幹細胞の放射線耐性機序に関する基礎的研究)

Koangyong Sung

HOKKAIDO UNIVERSITY

A study on radio-resistance mechanism of cancer stem-like cells using a property of low proteasome activity in canine tumor cell lines

---

A Dissertation for the Degree of Doctor of Philosophy

Koangyong Sung

Laboratory of Veterinary Surgery

Department of Veterinary Clinical Sciences

Graduate School of Veterinary Medicine

2022

Dissertation Examination Committee:

Professor Masahiro Okumura, Supervisor

Professor Takashi Kimura

Associate Professor Kenji Hosoya

Associate Professor Hironobu Yasui

Specially Appointed Assistant Professor Tatsuya Deguchi

A study on radio-resistance mechanism of cancer stem-like cells using a property of low proteasome activity in canine tumor cell lines

by

Koangyong Sung

A dissertation submitted to the Graduate School of Veterinary Medicine of Hokkaido University in fulfillment of the requirements for the degree of Doctor of Philosophy

Hokkaido University

Japan

2022

Table of Contents

Publications Related to the Dissertation

The contents of this dissertation are based on the following original publication listed below by their Roman numeral I of the research conducted during the period April 2018 – March 2022.

I. **Sung, K.**, Hosoya, K., Murase, Y., Deguchi, T., Kim, S., Sunaga, T. and Okumura, M. 2021. Visualizing the cancer stem-like properties of canine tumour cells with low proteasome activity. Vet. Comp. Oncol. In press. doi: 10.1111/vco.12779.

List of Abbreviations

53BP1	p53-binding protein 1
ABC	ATP-binding cassette
ABCB1	ATP-binding cassette sub-family B member 1
ABCB5	ATP-binding cassette sub-family B member 5
ABCC1	ATP-binding cassette sub-family C member 1
ABCG2	ATP-binding cassette sub-family G member 2
ANOVA	Analysis of variance
bFGF	Basic fibroblast growth factor
BSA	Bovine serum albumin
CDS	Coding sequence
cODC	Carboxyl-terminal degron of ornithine decarboxylase
DAPI	4’,6-diamidino-2-phenylindole
DI	DNA index
DIC	Differential interference contrast
DMARD	Disease-modifying antirheumatic drug
DMEM	Dulbecco's Modified Eagle Medium
DSB	DNA-double strand break
EDTA	Ethylenediaminetetraacetic acid
EGF	Epidermal growth factor
FBS	Fetal bovine serum
FCCP	Carbonyl cyanide 4-(trifluoromethoxy)phenylhydrazone
FITC	Fluorescein isothiocyanate

FPKM	Fragments per kilobase of transcript per million
GFP	Green fluorescent protein
GSH	Glutathione
Gy	Gray
H&E	Hematoxylin and eosin
HRP	Horseradish peroxidase
kDa	Kilodaltons
LET	Low-linear energy transfer
mRNA	Messenger ribonucleic acid
NADPH	Nicotinamide adenine dinucleotide phosphate
NFYA	Nuclear transcription factor Y subunit alpha
NFκB	Nuclear factor kappa B
NHEJ	Non-homologous end-joining
OCR	Oxygen consumption rate
Oct-4	Octamer-binding transcription factor 4
PBS	Phosphate-buffered saline
PCR	Polymerase chain reactions
PVDF	Polyvinylidene difluoride
RNA	Ribonucleic acid
ROS	Reactive oxygen species
RPMI	Roswell Park Memorial Institute medium
RT-qPCR	Reverse transcription-quantitative polymerase chain reactions

SD	Standard deviation
SDS-PAGE	Sodium dodecyl sulfate-polyacrylamide gel electrophoresis

List of Figures

List of Tables

GENERAL INTRODUCTION

Local recurrence by survived tumor cells still presents problems in radiation therapy. The recurrence after treatment is promoted by radio-resistance of tumors, and the radio-resistance should be solved for an effective tumor eradiation [Sato *et al*., 2019; Li *et al*., 2016]. Increasing results which could explain that tumors were initiated from a small distinct population having resistance to therapeutics like radiation therapy established a hypothesis of cancer stem cells (CSCs) [Pinho *et al*., 2012; Li *et al*., 2016]. The term 'cancer stem cells' was firstly suggested by researchers who reported the existence of CSCs which would have tumor-initiating potential in hematological cancer cells [Bonnet and Dick, 1997]. The special subpopulation exhibited self-renewal, differentiation capacity, expression of genes promoting tumor development represented as CSC markers, and tumorigenic potential [Batlle and Clevers, 2017]. Afterward, the CSC hypothesis has been taken in solid tumors, and the first evidence of CSCs was observed in human breast cancer [Al-Hajj et al., 2003]. Then, the existence of CSCs has been reported in many human solid tumors such as brain tumor [Singh *et al*., 2004], prostate tumor [Collins *et al*., 2005], nasopharyngeal tumor [Shen *et al*., 2015], hepatocellular carcinoma [Yin *et al*., 2007], melanoma [Quintana *et al*., 2008], osteosarcoma [Kamal *et al*., 2018], and so on. Also, CSC marker (Oct-4) positive cells in canine tumors were firstly identified in 2007 [Webster *et al*., 2007]. At the same time, canine osteosarcoma cells having a primitive phenotype were isolated using a sphere culture method *in vitro* [Wilson et al., 2007]. Thereafter, increasing evidence of canine CSCs has been reported, including resistance to cancer therapeutics, tumorigenic capacity, and poor prognosis [Rogez et al., 2019; Costa et al., 2019; Kishimoto et al., 2017; Tanabe et al., 2016]. The most significant property of CSCs is their resistance to tumor therapeutics like chemotherapy and radiation therapy. Therefore, survived CSCs contribute to tumor recurrence, and this indicates

that CSCs are potential therapeutic targets for complete elimination of tumor cells [Basu-Roy *et al*., 2013; Batlle and Clevers, 2017; Lathia *et al*., 2020].

Isolation of CSCs in both humans and canine is still difficult and should be overcome for establishing strategy to target CSCs. Several methods for isolation of CSCs have been tried like sphere formation and side population. Sphere formation was firstly suggested using neurocytes in 1992 [Reynolds and Weiss, 1992]. Sphere formation method is based on a principle that normal cells cannot survive when they are detached from extracellular matrix, undergoing a programmed cell death which is called anoikis [Frisch and Francis, 1994], but stem cells can survive as they require cell to cell interaction only [Reynolds and Weiss, 1992]. In addition, spheroid cells derived from stem cells have exhibited increased expression of CSC markers, viability, and tumorigenic capacity [Kim *et al*., 2012; Cao *et al*., 2011; Jagust *et al*., 2020]. Spheroid cells as a representative of CSCs have been used for research on CSCs [Salerno *et al*., 2013]. However, because of low ratio of the CSCs in spheroid cells, sphere formation method is still not satisfactory [Ma *et al*., 2011; Shen *et al*., 2015; Ning *et al*., 2016]. Another method for isolation of CSCs, side population, was reported in 1996 using murine hematopoietic stem cells and Hoechst 33342 dye [Goodell *et al*., 1996]. Tumour cells overexpressing ABCG2 transporter, which is an efflux Hoechst 33342 dye, are called side population. In flow cytometry analysis, they were negatively stained by Hoechst 33342 dye and located on the side of positively stained tumour cells. As the side population exhibited chemoresistance and CSC-like properties, side population assay or Hoechst 33342 efflux assay has been employed in CSC research [Ferletta *et al*., 2011; Begicevic and Falasca, 2017]. Nevertheless, because of low detection rate of CSCs in tumor cells, side population is still not satisfactory for CSC research [Patrawala *et al*., 2005].

The proteasome is a large protein complex having proteolytic function, and the proteolytic function of proteasome works with three main activities, including chymotrypsin-

like, caspase-like, and trypsin-like activities [Tanaka, 2009]. One of major objectives of proteasome is to maintain homeostasis of cells by degrading proteins related to apoptosis, cell cycle, transcription factors, and cell signaling. Degradation of these proteins by proteasome activities is performed in ubiquitin-dependent or ubiquitin-independent manners [Adams, 2003; Tanaka, 2009]. According to recent studies, CSCs have low proteasome activity [Vlashi *et al*., 2013; Tamari *et al*., 2014]. Low level of proteasome activity in CSCs would be linked to transcriptional and post-translation controls, which could affect proteasome sub-units [Lagadec *et al*., 2014a; Voutsadakis, 2017]. Low proteasome activity in CSCs retains cancer stemness by stabilising CSC related proteins, such as Oct-4, Sox-2, Nanog and Klf4, as they are proteasome substrates [Chen *et al*., 2005; Deng *et al*., 2020]. By using the low proteasome activity of CSCs, visualization of CSCs was established in human glioma and breast cancer cells in 2009 [Vlashi *et al*., 2009]. This system provides advantages of tracking CSCs in real time and simple isolation of CSCs both *in vitro* and *in vivo* conditions. ZsGreen1 fluorescent protein and ubiquitin-independent proteasome degron (carboxyl-terminal degron of ornithine decarboxylase: cODC) were employed in this system. Tumor cells were genetically engineered to express ZsGreen1 fluorescence which is fused to cODC. As cODC was directly degraded by proteasome activity, ZsGreen1 fluorescent proteins were accumulated at low proteasome activity of CSCs [Vlashi *et al*., 2009]. In human CSC research, visualization of CSCs has been reported in various tumor cells, such as lung cancer [Pan *et al*., 2010], pancreatic cancer [Furuyama *et al*., 2016], prostate carcinoma [Brush *et al*., 2009], head and neck cancer [Lagadec *et al*., 2014b], colorectal cancer [Munakata *et al*., 2016], and osteosarcoma [Tamari *et al*., 2014]. However, application of this CSC visualization in canine tumor cells has not well documented yet.

Radio-resistance is implicated to tumor recurrence and poor prognosis of radiation therapy [Olivares-Urbano *et al*., 2020]. As previously described, the radio-resistance of CSCs

must be overcome for complete tumor treatment [Rycaj and Tang, 2014]. Theoretically, CSCs can be eliminated with enough high dose of radiation therapy, but practical dose of radiation is limited by concurrent adverse effects on normal tissues in clinical use for patients who receive a course of radiation therapy [Delaney *et al*., 2005]. Therefore, understandings of intrinsic radio-resistance mechanism in CSCs is essential to reveal molecular targets of CSCs [Olivares-Urbano *et al*., 2020]. Some research reports that CSCs undergo low oxidative damage, which is a primary effect of low-linear energy transfer (LET) radiation like X-ray and gamma ray because, CSCs would have high expression levels of reductants like glutathione (GSH) [Rycaj and Tang, 2014].

Glutathione, which is the richest ubiquitous antioxidant, is one of intracellular thiol substances and protects cells from oxidative damage by reacting with electrophiles or reactive oxygen species (ROS). Synthesis of GSH follows a chain of enzymatic reaction and this needs three major compounds, which are cysteine, glutamate, and glycine [Ribas *et al*., 2014]. Cysteine is a rate-limiting molecule in the synthesis of GSH and can play a role of antioxidant [Stipanuk *et al*., 2006]. Cysteine can be synthesized by intracellular biosynthesis or decomposition of proteins, but cancer cells largely depend on cystine transporter xCT (SLC7A11) to obtain sufficient cysteine. Cystine transporter xCT imports extracellular cystine and the cystine is transformed to cysteine by a reduction reaction using NADPH for synthesis of GSH [Trachootham *et al*., 2009; Chio and Tuveson, 2017; Stipanuk *et al*., 2006; Combs and Denicola, 2019]. According to previous studies, xCT inhibition or knock down effectively breaks the redox balance of tumor cells by decreasing GSH synthesis [Nagane *et al*., 2018; Ye *et al*., 2014]. Sulfasalazine is a disease-modifying antirheumatic drug (DMARD) and now well-established for treatment of rheumatoid arthritis. Because of many beneficial points such as low cost, safety, and accessibility, sulfasalazine has been the first-line treatment for the rheumatoid arthritis [Plosker and Croom, 2005]. Sulfasalazine has also been

used frequently for treatment of intestinal diseases in dogs [German *et al*., 2010]. At the first time, effects of sulfasalazine on the xCT were reported in 2001 [Gout *et al*., 2001]. Inhibition of xCT by sulfasalazine shows antitumor effects that would induce non-apoptotic cell death, ferroptosis. The relation between cystine deprivation through xCT inhibition and ferroptosis was reported in 2012 [Dixon *et al*., 2012]. Ferroptosis is a kind of iron-dependent regulated cell death as a result of over-accumulation of lipid peroxidation [Gan, 2019]. Sulfasalazine decreases GSH contents through xCT inhibition and impedes detoxification of lipid peroxides inducing ferroptosis. In addition, xCT inhibition by sulfasalazine activates apoptotic pathway by increasing ROS level which is related to the effect of radiation therapy as described previously [Koppula *et al*., 2021]. Furthermore, sulfasalazine sensitizes CD133-positive CSCs with high level of GSH to anticancer therapies [Song *et al*., 2017], and sulfasalazine sensitizes CD44v-positive CSCs to anticancer agents in which CD44v stabilizes xCT on the cell membrane [Thanee et al., 2021]. Thus, with proved efficacy and safety [Xiao and Meierhofer, 2019], sulfasalazine would be an appropriate candidate for a radiosensitizer of CSCs.

The present study consists of two chapters. In the first chapter, canine tumor cells with low proteasome activity were imaged and isolated, subsequently demonstrating their CSC-like properties. In second chapter, by using the CSC visualization system, radio-resistance of the canine tumor cells with low proteasome activity was evaluated, and the radio-resistance mechanism was revealed based on GSH contents mainly. Furthermore, following results, radiosensitizing effects of sulfasalazine were investigated for targeting CSCs in radiation therapy.

CHAPTER I

Visualizing the cancer stem-like properties of canine tumor cells with low proteasome activity

INTRODUCTION

Cancer stem cells, which occupy small percentage of tumor cells, are neoplastic counterparts of normal tissue stem cells, representing self-renewal capacity and generation of differentiated cells [Batlle and Clevers, 2017]. The small subpopulation of tumor cells has resistance to conventional tumor treatments, thus surviving CSCs cause tumor recurrence [Basu-Roy *et al*., 2013]. To eradicate tumor cells, CSCs have received attention in terms of potential therapeutic targets [Batlle and Clevers, 2017; Lathia *et al*., 2020].

Canine CSCs also comprise a small fraction of entire tumour cells with some variation across tumour cell types and methods for identifying CSCs [Michishita *et al*., 2011; Ferletta *et al*., 2011; Nemoto *et al*., 2011; Wilson *et al*., 2008]. Furthermore, the existence of canine CSCs is associated with therapy resistance, malignancy grade and poor prognosis, such as that of human CSCs [Rogez *et al*., 2019; Costa *et al*., 2019; Kishimoto *et al*., 2017; Tanabe *et al*., 2016]. However, outcomes of therapies targeting CSCs are still not satisfied in both human and canine tumors.

In canine CSC research, because of the lack of methods and limited available CSC markers, the identification and isolation of CSCs have faced difficulties. As spheroid cells have higher percentage of CSCs than adherent cells, sphere formation assay has been used for CSC research [Salerno *et al*., 2013], but it is still limited by the low ratio of CSCs in spheroid cells [Ma *et al*., 2011; Shen *et al*., 2015; Ning *et al*., 2016]. A subset of cancer stem cells, termed as side population cells which efflux Hoechst 33342 dye mediated by the ABCG2 transporter, has been used for CSC research [Nemoto *et al*., 2011; Ferletta *et al*., 2011]. However, employment of the side population cells is also limited, because only 30% of human tumor cell lines express the function of ABCG2 transporter [Patrawala *et al*., 2005].

Proteasome, a principal multi-subunit protease, is responsible for the degradation of

intracellular proteins with three peptidase activities (chymotrypsin-like, caspase-like, and trypsin-like activities) [Tanaka, 2009]. Thus, the function of proteasome play an important role for keeping cellular processes constantly by the degradation of unnecessary proteins [Collins and Goldberg, 2017]. In tumor cells, proteasome-mediated degradation of proteins like p53, p27, β-catenin, and NFκB is related to cell proliferation, metastasis, survival, and resistance to tumor therapies [Jang, 2018; Crawford *et al*., 2011]. In addition, the proteasome activity in CSCs is down-regulated by over-expressing Musashi-1 that inhibits NF-YA activity [Lenos and Vermeulen, 2016], a transcription factor regulating proteasome subunit expression [Xu *et al*., 2012]. The low proteasome activity in CSCs cannot degrade CSC marker-related proteins like Notch intracellular domain, thereby promoting CSC phenotype [Lagadec *et al*., 2014a].

In CSC research, a system visualizing CSCs had lately been established in various types of human tumors based on the difference of proteasome activity between CSCs and non-CSCs [Vlashi *et al*., 2013; Tamari *et al*., 2014]. In this visualizing system, tumor cells were genetically modified to express fluorescence protein, ZsGreen1, connected with ubiquitin-independent proteasome degron (cODC). As cODC is degraded by proteasome and CSCs possess lower proteasome activity than non-CSCs, ZsGreen1 proteins were accumulated in CSCs, resulted in the emission of the ZsGreen1 fluorescence [Adikrisna *et al*., 2012]. Interestingly, visualized tumor cells had higher radio-resistance or chemo-resistance than non-visualized tumor cells [Della Donna *et al*., 2012; Hayashi *et al*., 2014] indicating the possibility of this system as a research tool for establishing new strategies to eradicate CSCs.

In canine tumor research, the biological changes in the CSCs can be investigated in real-time *in vitro* and *in vivo* by visualizing the CSCs. This study aimed to establish a visualization system for canine CSCs. Here canine osteosarcoma and canine transitional cell carcinoma expressing ZsGreen1-cODC were established to visualize tumor cells with low

proteasome activity. Moreover, the connection between CSC-like properties and low proteasome activity was revealed.

MATERIALS AND METHODS

Cell line validation and culture condition

Canine cell lines HMPOS (osteosarcoma) [Barroga *et al*., 1999], MegTCC (transitional cell carcinoma) [Yamazaki *et al*., 2015; Takagi *et al*., 2005] and CMeC (melanoma) [Inoue *et al*., 2004] were established and have been used in previous canine tumor studies [Song *et al*., 2020; Deguchi *et al*., 2019; Enjoji *et al*., 2015]. HMPOS and CMeC were validated by RNA sequencing. Species of MegTCC was confirmed by the expression of canine cytochrome C oxidase I gene [Cooper *et al*., 2007]. HMPOS, MegTCC and CMeC were cultured in RPMI-1640 media (Gibco, Grand Island, NY, USA). Human embryonic kidney cell line (293T) was cultured in DMEM (Gibco) media. Both RPMI-1640 and DMEM media were supplemented with 10% fetal bovine serum (FBS) (Sigma-Aldrich, St. Louis, MO, USA), 100 units/mL of penicillin G (Wako Pure Chemical Industries, Osaka, Japan) and 100 μg/mL of streptomycin (Wako) at 37°C and 5% CO_2.

Construction of ZsGreen1-cODC-expressing stable cell lines

A lentiviral vector containing ZsGreen1-*cODC* was prepared (Figure I-1A-C). The canine *cODC* sequence encoding 51 amino acids at the C-terminus was amplified from the cDNA from CMeC cells and KOD -plus- ver. 2 (Toyobo, Osaka, Japan) using specific primers (Table I-1) and PCR conditions (Table I-2). The PCR fragment was cloned into pZsGreen1-C1 (TaKaRa, Kusatsu, Japan) at the C-terminus of ZsGreen1. Then, a fragment containing ZsGreen1 and the canine cODC were cloned into the lentiviral vector CSII-CMV-MCS-IRES2-Bsd (Riken BRC, Tsukuba, Japan).

The lentiviral vector and packaging plasmids were transfected into 293T cells for 48

hours using Lipofectamine 3000 (Invitrogen, Carlsbad, CA, USA) following the manufacturer's protocol. The supernatant was filtered through 0.2 μm pore-diameter cellulose acetate membrane filters (Advantec Toyo Ltd, Tokyo, Japan), and the lentiviral particles were concentrated using Lenti-X concentrator (TaKaRa). HMPOS and MegTCC cells were infected with the lentiviral supernatant and cultured in RPMI-1640 with 10% FBS and 10 μg/mL blasticidin (Wako) to select for single-cell clones. ZsGreen1-cODC expression was confirmed by treating the cells overnight with 0.5 μM of MG-132 (Sigma-Aldrich), which is a potent inhibitor of chymotrypsin like-proteasome activity [Mroczkiewicz *et al*., 2010]. The fluorescence intensity of ZsGreen1 was detected *via* fluorescence microscopy and flow cytometry.

Sphere formation assay

Spheroids were cultured [Deguchi *et al.*, 2019] by seeding cells on ultra-low attachment six-well plates (Corning, Corning, NY, USA) at various densities in FBS-free Dulbecco's Modified Eagle Medium (DMEM)/F12 (Wako) with 20 ng/mL of human recombinant EGF, 10 ng/mL of human recombinant basic FGF (Wako), 100 units/mL of penicillin, 200 mg/mL of streptomycin and 0.4% bovine serum albumin (Invitrogen). Growth factors, 1 ng/mL of EGF and bFGF each, were added every 24 hours. After 14 days, spheroids with a diameter of 50 μm were harvested.

Proteasome activity assay

Chymotrypsin-like proteasome activity was evaluated using a Proteasome-Glo™ Chymotrypsin-Like Cell-Based Assay (Promega, Tokyo, Japan). Cells were seeded at 10^4 cells/well in a white-walled 96-well plate (Corning), allowed to attach for 2 hours in a humidified chamber at 37°C and 5% CO_2 and equilibrated at 22°C for 30 minutes.

Luminescence at 10 minutes after the addition of the Proteasome-Glo^{TM} cell-based reagent was detected using a microplate reader (Infinite 200, Tecan Japan, Kanagawa, Japan).

Flow cytometry and cell sorting

HMPOS-ZsG or MegTCC-ZsG cells grown to the log phase were washed with phosphate-buffered saline (PBS), trypsinized with 0.025% trypsin-EDTA, suspended and analysed on a FACSVerse flow cytometer (BD Biosciences, San Jose, CA, USA) or sorted on a FACSAria II flow cytometer (BD Biosciences). The cancer cells were defined as ZsG^+ if their fluorescence intensity was higher than that of the untransfected parental cells.

Time-lapse analysis

After sorting, 1.20×10^4 ZsG^+ cells were plated on a 35-mm glass-bottom dish (Matsunami, Tokyo, Japan) in the culture medium and then allowed to attach to the glass bottom for 2 hours at 37°C and 5% CO_2. Subsequently, the cells were placed in a stage-top incubator (INUBG2TF-WSKM, Tokai Hit, Shizuoka, Japan), which maintained a constant temperature of 37°C, 5% CO_2. Differential interference contrast (DIC) images and ZsGreen1 fluorescence images of the live cells were photographed at 30-min intervals for 48 hours under an ECLIPSE Ti-E microscope (Nikon, Tokyo, Japan) equipped with a Plan Apo VC 20×/0.75 NA objective lens (Nikon), GFP/FITC filter-cube (Semrock, Rochester, NY, USA), BI XY stage (Chuo Precision Industrial Co. Ltd., Tokyo, Japan) and Zyla 5.5 sCMOS camera (Oxford Instruments, Abingdon, UK). Additionally, the microscope's focus was managed using a Perfect Focus System (Nikon), while acquiring the images. DIC images were captured with 50-ms exposures, and ZsGreen1 fluorescence images were captured with

1,000-ms and 600-ms exposures in HMPOS-ZsG and MegTCC-ZsG, respectively. Finally, the images were converted to time-lapse videos using NIS-elements AR software (Nikon).

Cell cycle analysis

Cell cycle analysis was conducted [Schmid and Sakamoto, 2001] by plating 1×10^5 cells in a 10-cm dish to incubate for 3 days. Then, the cells were washed with PBS, trypsinized and centrifuged at 300 × g for 5 minutes at 4°C, resuspended with 500 μL of cold (4°C) PBS, fixed with an additional 500 μL of cold 2% paraformaldehyde (Wako) for 1 hour at 4°C, centrifuged at 300 × g and 4°C for 5 minutes and washed with cold PBS. The cell plasma membrane was permeabilised by resuspending the cells dropwise in 1 mL of 70% ethanol at −20°C, incubating for 4 hours at 4°C, centrifuging at 300 g for 5 minutes at 4°C and washing with cold PBS. The cells were then incubated in 1 mL of 40 μg/mL propidium iodide (Sigma-Aldrich) with 100 μg/mL of ribonuclease A for 30 minutes in a 37°C water bath under dark condition. Finally, the DNA contents of the cells were analysed using a FACSVerse flow cytometer (BD Biosciences).

RNA library preparation and sequencing

After sorting the ZsG^- and ZsG^+ cells, the total RNA was isolated using a RNeasy Micro Kit (Qiagen, Hilden, Germany) and sequenced by an external laboratory (DNAFORM, Yokohama, Japan). Bioanalyzer (Agilent Technologies, Forster City, CA, USA) was used to confirm the quality of the total RNA. The RNA integrity number of the samples was 10 (intact RNA). Poly(A) + RNA was enriched using the NEBNext Poly(A) mRNA Magnetic Isolation Module (New England BioLabs, Beverly, MA, USA). Double-stranded cDNA libraries (RNA-seq libraries) were generated using the SMARTer Stranded Total RNA

Sample Prep Kit (Clontech, Palo Alto, CA, USA). RNA-seq libraries were sequenced on a Nextseq 500 sequencer (Illumina, San Diego, CA, USA) with paired-end reads (50 nucleotides of read1 and 25 nucleotides of read2). The reads were mapped to the dog reference genome (CanFam3.1) using STAR (ver. 2.7.2b). The unique reads mapped to annotated genes were counted using featureCounts (ver. 1.6.1), and the FPKM values were calculated using the mapped reads normalised to the total counts and transcript. The differentially expressed genes were detected using DEseq2 (ver. 1.20.0).

Reverse-transcription quantitative PCR

Reverse-transcription quantitative PCR (RT-qPCR) was performed to evaluate the expression of cancer stem cell marker genes (CSC markers) in the ZsG^- and ZsG^+ cells. The total RNA was isolated using TRIzol (Invitrogen). Then, 500 ng of the total RNA was reverse-transcribed to cDNA using a M-MLV RT kit (Invitrogen). Next, qPCR was conducted using the KAPA SYBR® FAST qPCR Master Mix (2X) Kit (Kapa Biosystems, Woburn, MA, USA) and specific primers (Table I-1) to undergo initiation denaturation at 95°C for 2 minutes, 40 cycles of denaturation at 95°C for 15 seconds, annealing at 60°C for 20 seconds and extension at 72°C for 1 minutes. The DNA was quantified using Rotor-Gene Q Series Software ver. 2.3.1 (Qiagen).

Function of ABCG2 transporter

Hoechst 33342 dye (Sigma-Aldrich) efflux capacity mediated by the function of ABCG2 transporter was evaluated in ZsG^- and ZsG^+ cells. The staining method using Hoechst 33342 dye was carried out according to a previous study [Pan *et al*., 2010]. Then, the fluorescence intensity of Hoechst 33342 was measured by FACSAria II flow cytometer (BD Biosciences).

Tumorigenicity assay

The cancer cells were sorted into ZsG^- and ZsG^+ cells using the FACSAria II cell sorter (BD Biosciences). The number of cells was adjusted to $1 \times 10^1 – 1 \times 10^4$ cells/50 μL PBS, mixed with 50 μL of Matrigel (BD Biosciences) and injected subcutaneously into the left flank region of 7-week-old female BALB/cAJc1-*nu/nu* mice (CLEA Japan, Inc., Tokyo, Japan). Afterwards, the tumors were measured [Tumor volume = (length) × $(\text{width})^2/2$] daily. At the endpoint, the mice were euthanized according to the guidelines of Hokkaido University Institutional Animal Care and Use Committee (Approval Number: 20-0049). The tumor tissues were fixed in 4% paraformaldehyde, paraffinized, sliced into 3-μm-thick sections and stained with H&E or DAPI (Invitrogen). The periphery, core and necrotic core tumor regions were defined based on our observation of the H&E-stained sections according to a previous study [Wang *et al*., 2015]. In each region, the ZsG^+ cells were counted under a fluorescence microscope to calculate the fraction of the ZsG^+ cells.

Statistical analysis

The data was analysed using IBM SPSS Statistics version 26.0 (IBM, Armonk, NY, USA) and expressed as mean ± standard deviation (SD) with a 95% confidence interval. The Shapiro–Wilk test was used to assess the normality of the data. The homogeneity of variance was evaluated using Levene's test, and data were directly compared using Student's *t*-test. The data were analysed *via* one-way analysis of variance (ANOVA), followed by Tukey's multiple comparison tests for multiple comparisons. The data were considered statistically significant if the *p*-value was less than 0.05 (**p*), 0.01 (***p*) or 0.001 (****p*).

RESULTS

Construction of cancer cell lines expressing ZsGreen1-cODC

The 156-bp sequence of amplified canine *cODC*, confirmed to be identical to that in the database, was inserted into the C-terminal region of the ZsGreen1 gene with a five-amino acid bridge (Figure I-2). A few cells with ZsGreen1 fluorescence were observed at 2.67 ± 0.58% and 3.00 ± 1.73% for the HMPOS-ZsG and MegTCC-ZsG cells, respectively (Figure I-3A). The ratio of the ZsG^+ cells was significantly increased by treatment with MG-132, confirming the mode of the visualization system (Figure I-3B).

Applicability of the visualization system to canine CSCs

The spheroid cells derived from the constructed cells exhibited enrichment at 13.64 ± 0.42% and 14.22 ± 2.19%, respectively, of the HMPOS-ZsG and MegTCC-ZsG cells compared with 2.00 ± 0.36% and 3.32 ± 0.97%, respectively, of the adherent HMPOS-ZsG and MegTCC-ZsG cells (Figure I-4A-B). As CSC visualization is based on proteasome activity, the chymotrypsin-like proteasome activity was evaluated in the spheroid cells exhibiting CSC-like properties [Deguchi *et al.*, 2019]. The HMPOS and MegTCC-derived spheroid cells demonstrated lower chymotrypsin-like proteasome activity than the adherent cells (Figure I-4C), indicating that proteasome activity-based visualization was feasible for HMPOS and MegTCC cells.

Cancer stem-like properties

Cell division was evaluated *via* time-lapse analysis after sorting the ZsG^+ cells. Symmetric divisions with or without phenotype change, indicated by the change in ZsGreen1

fluorescence intensity, as well as asymmetric divisions were observed in the ZsG^+ cells of the HMPOS-ZsG and MegTCC-ZsG cells (Figure I-5A). Among the HMPOS-ZsG cells, symmetric divisions with or without phenotype change and asymmetric divisions were 76.00 ± 1.00%, 19.67 ± 0.58% and 4.33 ± 1.15%, respectively. Among the MegTCC-ZsG cells, symmetric divisions with or without phenotype change and asymmetric divisions were 39.67 ± 1.15%, 54.67 ± 4.51% and 5.67 ± 3.51%, respectively. These results were further supported by the observed differentiation capacity of the ZsG^+ cells. After 3 days of incubation, the ratio of the ZsG^+ cells in sorted ZsG^- cells and ZsG^+ cells groups was measured using FACS. In both the HMPOS-ZsG and MegTCC-ZsG cells, the ratio of the ZsG^+ cells was not changed significantly in the sorted ZsG^- cells group, but in the sorted ZsG^+ cells group, the ratio of ZsG^+ cells significantly decreased, indicating the increased ratio of the ZsG^- cells (HMPOS-ZsG, 98.13 ± 3.23% to 9.17 ± 1.01%; MegTCC-ZsG, 92.50 ± 7.71% to 22.48 ± 2.81%) (Figure I-6).

The division of the ZsG^+ cells was examined using cell cycle analysis. The ZsG^+ cells had a low percentage of G0/G1 phase cells in the HMPOS-ZsG cells, at 69.27 ± 2.47% and 55.85 ± 2.67% for the ZsG^- and ZsG^+ cells, respectively ($p = 0.003$), and in the MegTCC-ZsG cells, at 68.96 ± 0.44% and 59.15 ± 0.69% for the ZsG^- and ZsG^+ cells, respectively ($p = 0.000$). The ZsG^+ cells had a high percentage of S phase cells in the HMPOS-ZsG cells (13.02 ± 1.96% and 21.29 ± 1.64% for the ZsG^- and ZsG^+ cells, respectively, $p = 0.005$), and MegTCC-ZsG cells (12.56 ± 1.46% and 16.72 ± 1.82% for the ZsG^- and ZsG^+ cells, respectively, $p = 0.037$). Meanwhile, the ZsG^+ and ZsG^- cells had similar percentages of G2/M phase cells in the HMPOS-ZsG cells, at 16.92 ± 3.00% and 20.96 ± 1.65% for the ZsG^- and ZsG^+ cells, respectively ($p = 0.111$). However, in the MegTCC-ZsG cells, the ZsG^+ cells had a higher percentage of G2/M phase cells, at 22.98 ± 1.24%, than the ZsG^- cells, at 17.78 ± 1.94% ($p = 0.017$) (Figure I-5B).

The expression of CSC markers was revealed using RNA sequencing in the ZsG^- and ZsG^+ cells in the HMPOS-ZsG cells. Among the CSC markers expressed in the ZsG^- and ZsG^+ cells, *CD133* (Log2 fold change, 4.664), *CD200* (5.104) and *KRT14* (6.220) were upregulated in the ZsG^+ cells (Figure I-5C). Then, the expression of CSC markers, *CD133*, *CD200*, *KLF4*, *DPP4*, *CD44*, *CD9*, *Thy1* and *MCAM*, in the ZsG^- and ZsG^+ cells were analysed. Several CSC markers, including *CD133* ($p = 0.005$), *KLF4* ($p = 0.032$) and *CD9* ($p = 0.024$) in the HMPOS-ZsG cells and *CD133* ($p = 0.030$), *CD44* ($p = 0.030$) and *Thy1* ($p = 0.035$) in the MegTCC-ZsG cells, were upregulated in the ZsG^+ cells (Figure I-5D).

Function of ABCG2 transporter was evaluated using Hoechst 33342 dye. In HMPOS-ZsG cells, ZsG^+ cells showed lower fluorescence intensity of Hoechst red than ZsG^- cells, indicating higher function of ABCG2 transporter. However, in MegTCC-ZsG cells, there was no difference in the fluorescence intensity of Hoechst red between ZsG^- cells and ZsG^+ cells (Figure I-7).

Tumorigenicity

The ZsG^- and ZsG^+ cells of the HMPOS-ZsG and MegTCC-ZsG cells were sorted and injected into the mice to evaluate their *in vivo* tumorigenic capacity. In each group, six mice were injected with 1×10^1 or 1×10^2 HMPOS-ZsG cells or 1×10^3 or 1×10^4 MegTCC-ZsG cells per inoculum.

In the HMPOS-ZsG group, all six mice receiving 1×10^1 ZsG^+ cells formed tumors with a mean volume of 1,219.35 ± 1,175.20 mm^3 68 days following inoculation. In the group receiving 1×10^2 cells, three of the six mice injected with ZsG^- cells formed tumors with a mean volume of 496.83 ± 376.28 mm^3, and all of the six mice injected with ZsG^+ cells formed tumors with the mean volume of 1,376.76 ± 662.65 mm^3 ($p = 0.037$) 29 days following inoculation. Among the mice injected with ZsG^+ cells, one had abdominal

metastasis.

No tumor was formed in the MegTCC-ZsG group receiving 1×10^3 ZsG^- or ZsG^+ cells. At 99 days following inoculation with 1×10^4 cells, none of the mice injected with the ZsG^- cells and two of the six mice injected with ZsG^+ cells formed tumors with the mean volume of $1{,}899.36 \pm 412.19$ mm^3 (Figure I-8A-B). The formation of each tumor was confirmed *via* histopathological analysis, and ZsGreen1 fluorescence in the tumor sections was detected *via* fluorescence microscopy. In the HMPOS-ZsG group, the ZsG^+ cells were more widely distributed in the tumor sections derived from the ZsG^+ cells than those derived from the ZsG^- cells (Figure I-8C). Furthermore, the ratio of the ZsG^+ cells in various regions of the tumor (Figure I-9A) was different in the HMPOS-ZsG tumors, at $3.33 \pm 0.58\%$, $1.33 \pm 0.29\%$, $0.17 \pm 0.10\%$ and $11.83 \pm 1.04\%$ in the core, periphery, necrotic core and metastasis, respectively, and in the MegTCC-ZsG tumors, at $4.83 \pm 1.04\%$, $1.33 \pm 0.76\%$ and $0.17 \pm 0.50\%$ in the core, periphery and necrotic core, respectively, (Figure I-9B-C).

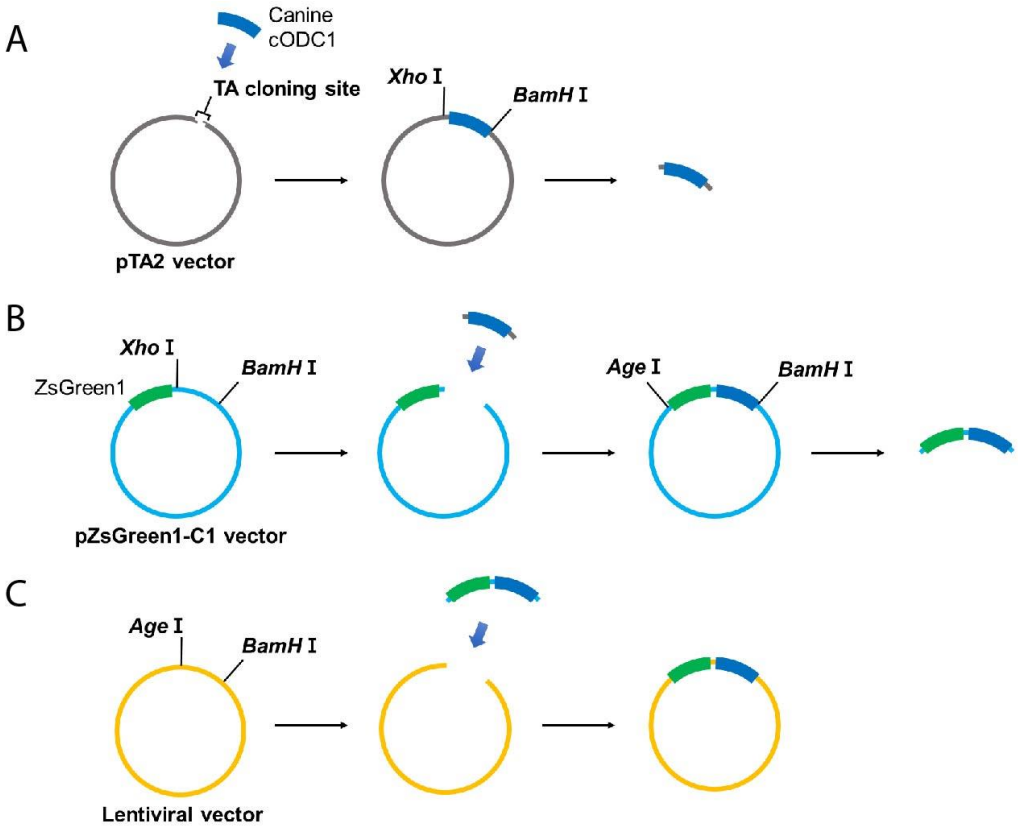

Figure I-1. Schematic diagram of the process of lentiviral vector construction

(A) Canine cODC1 was amplified and the fragment was subcloned into the pTA2 vector. (B) The canine cODC1 fragment was inserted into the multicloning site of the pZsGreen-C1 vector, which is next to the c-terminal of the ZsGreen1. (C) The digested fragment of ZsGreen1/canine cODC1 was inserted into the lentiviral vector (CSII-CMV-MCS-IRES2-Bsd), and this recombinant plasmid was used for lentiviral transfection.

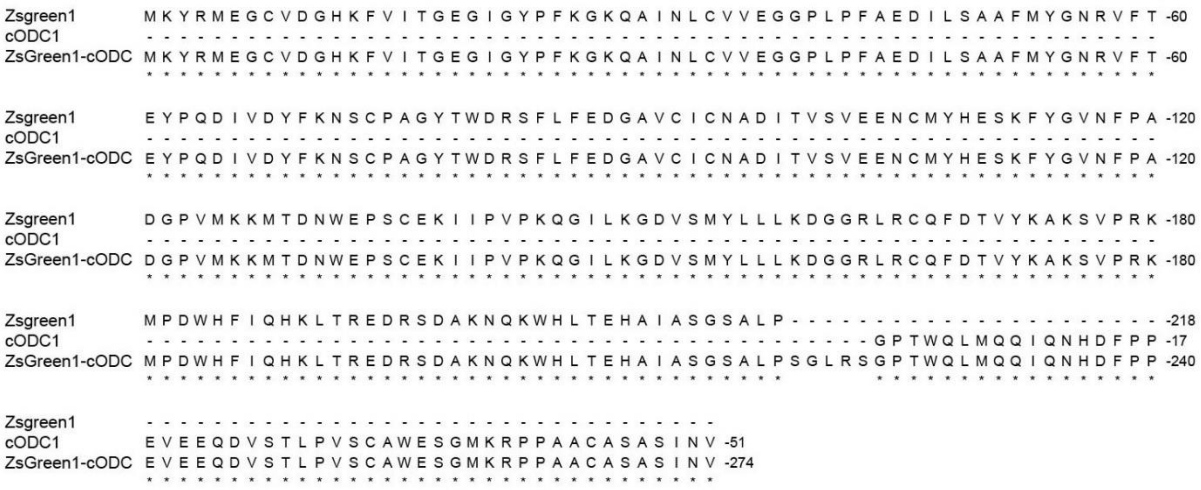

Figure I-2. Amino acid sequence of ZsGreen1-cODC

The amino acids sequence of ZsGreen-cODC was inserted to the lentiviral vector and the sequence was analyzed. The sequence of ZsGreen-cODC was aligned with predicted partial sequence of ZsGreen1 and full sequence of cODC1.

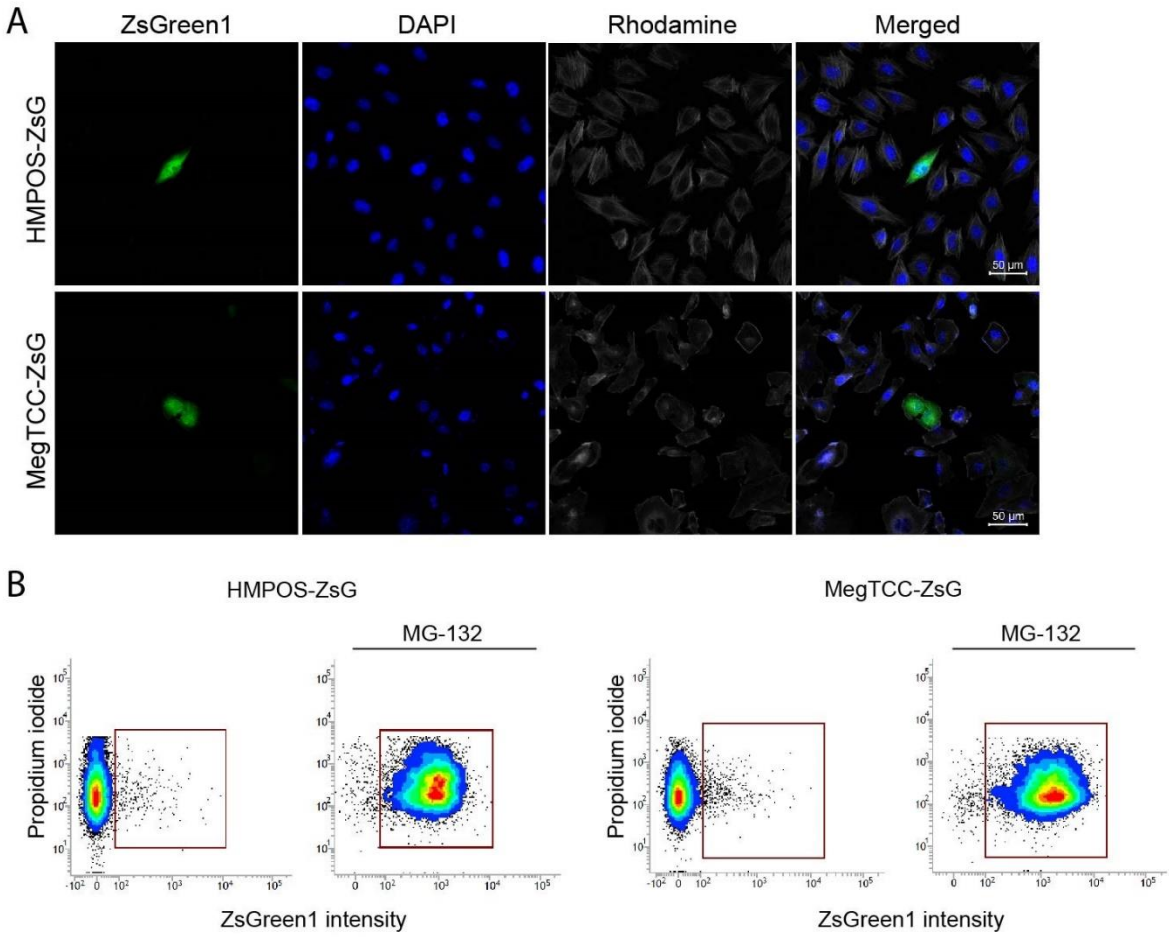

Figure I-3. Construction of cancer cell lines expressing ZsGreen1-cODC

(A) Adherent cells of HMPOS-ZsG and MegTCC-ZsG showing green fluorescent ZsG^{+} cells and other ZsG^{-} cells. (B) Change of ZsGreen1 fluorescence intensity after incubating cancer cells with 0.5 μM of MG-132 for 12 hours. Propidium iodide was used for screening dead cells.

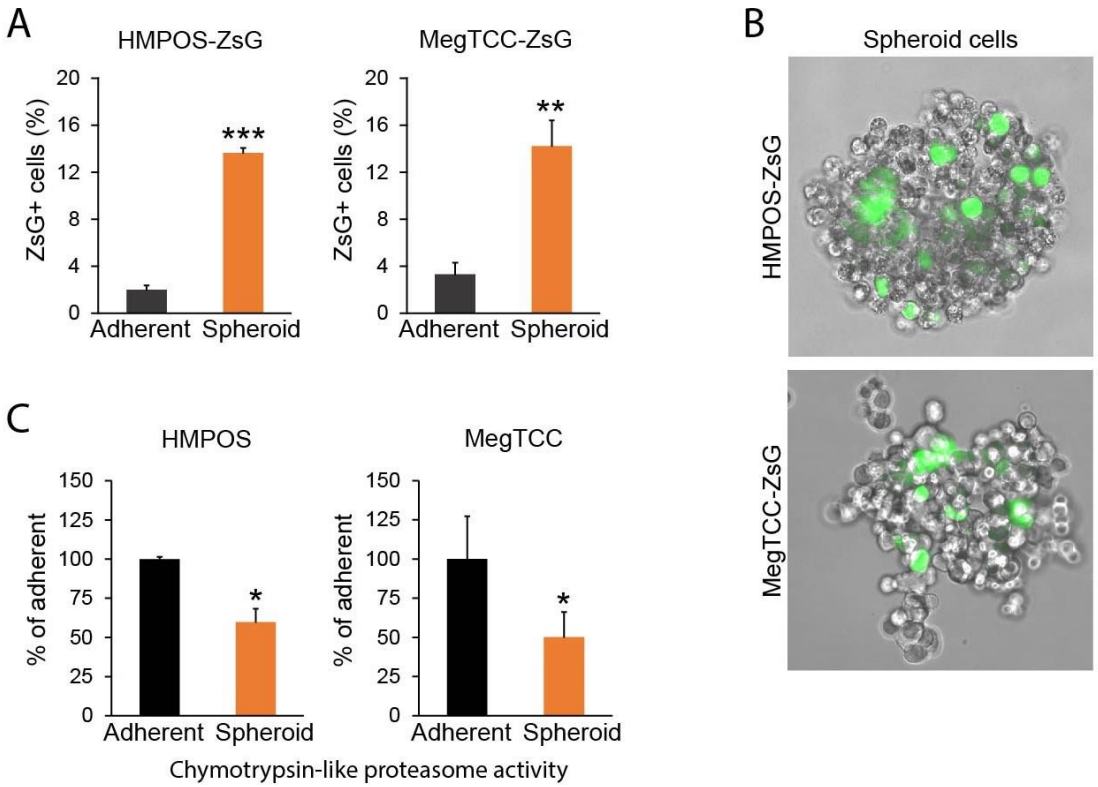

Figure I-4. Ratio of ZsG$^+$ cells after sphere formation and chymotrypsin-like proteasome activity in adherent and spheroid cells

(A) Ratio of ZsG$^+$ cells in adherent and spheroid cells. (B) Green fluorescent ZsG$^+$ cells within spheroid cells in HMPOS-ZsG and MegTCC-ZsG. (C) Chymotrypsin-like proteasome activity in adherent and spheroid cells. Luminescence intensity of proteasome activity is shown as relative value to adherent cells. Student's *t*-test was used for statistical analysis. *$p < 0.05$, **$p < 0.01$, and ***$p < 0.001$.

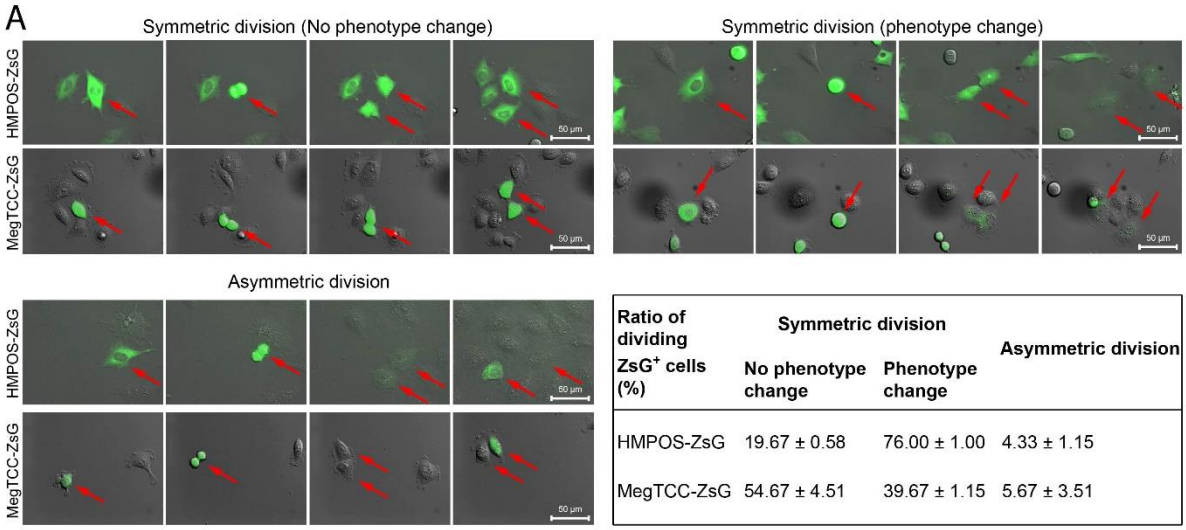

Ratio of dividing ZsG$^+$ cells (%)	Symmetric division		Asymmetric division
	No phenotype change	Phenotype change	
HMPOS-ZsG	19.67 ± 0.58	76.00 ± 1.00	4.33 ± 1.15
MegTCC-ZsG	54.67 ± 4.51	39.67 ± 1.15	5.67 ± 3.51

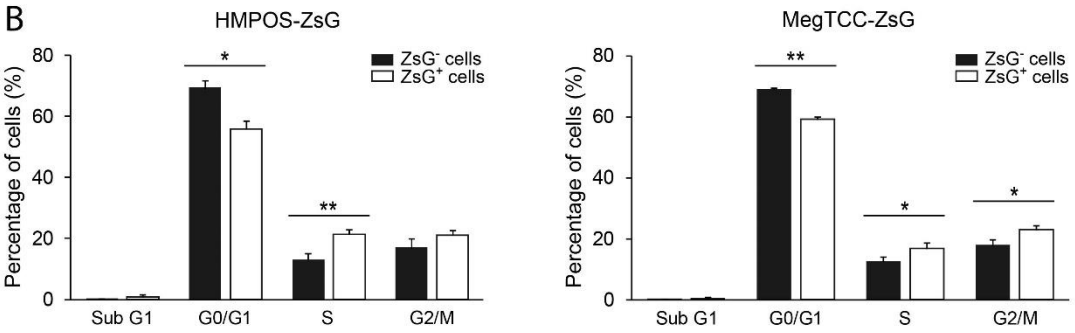

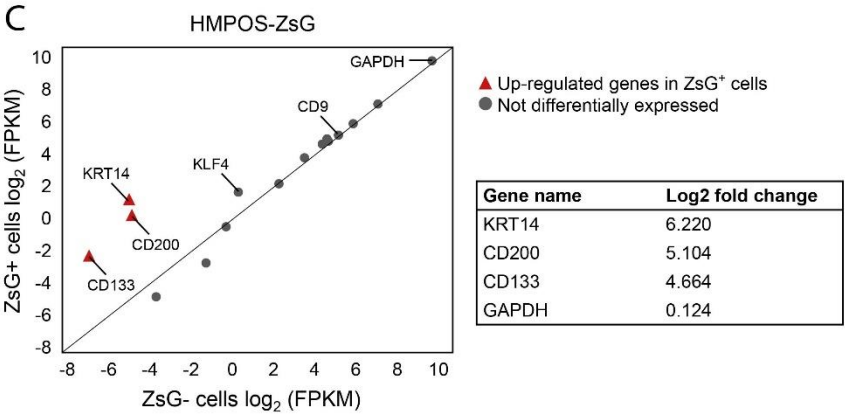

Gene name	Log2 fold change
KRT14	6.220
CD200	5.104
CD133	4.664
GAPDH	0.124

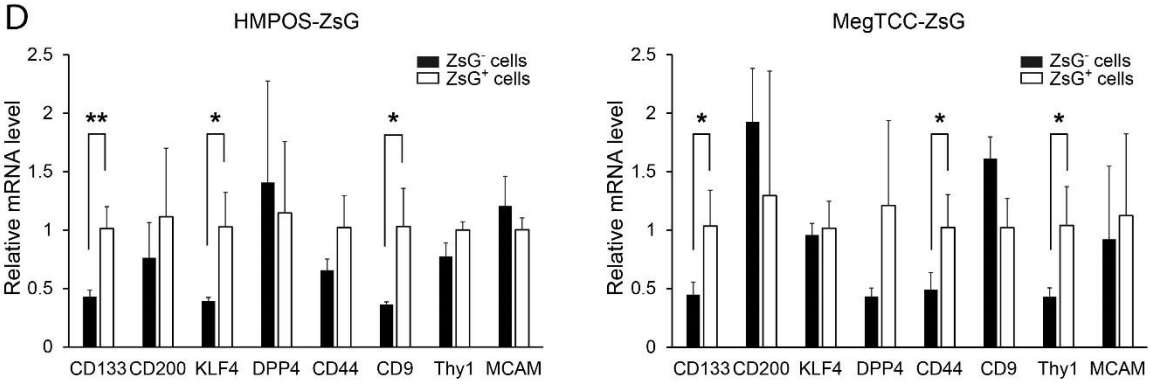

Figure I-5. Cancer stem-like properties

(A) Time-lapse images showing symmetric divisions with/without phenotype change and asymmetric divisions. Ratio of dividing ZsG^+ cells in different types of cell divisions. Data, mean ± SD. (B) Cell cycle analysis shown as percentage of cells (%) using propidium iodide. (C) The expression of CSC markers from RNA sequencing in HMPOS-ZsG. (D) Relative mRNA levels of CSC markers by RT-qPCR. HMPOS-ZsG and MegTCC-ZsG were used for the analyses. Student's *t*-test was used for statistical analysis. $*p < 0.05$ and $**p < 0.01$.

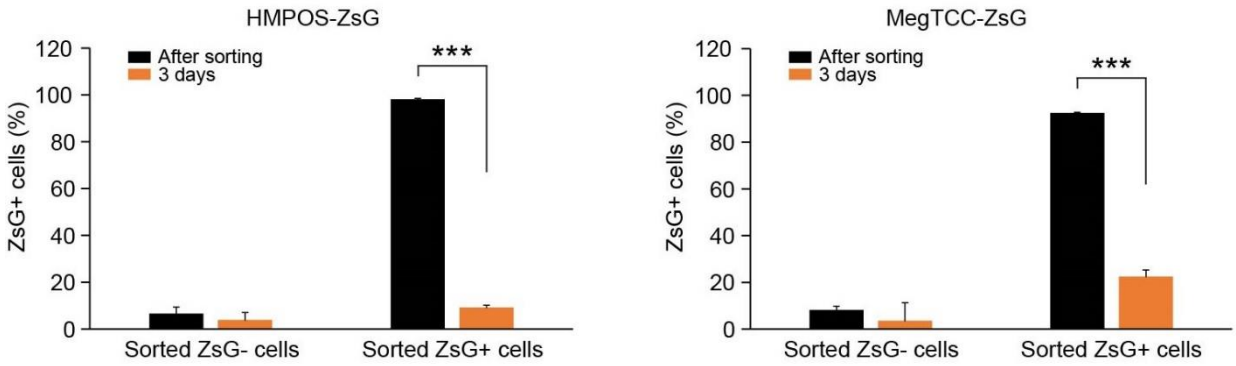

Figure I-6. Differentiation capacity

The changes of the ratio of ZsG^+ cells in sorted ZsG^- cells and ZsG^+ cells groups after 3 days of incubation. HMPOS-ZsG and MegTCC-ZsG were used for the analyses. Tukey's multiple comparison test was used for statistical analysis. ***$p < 0.001$.

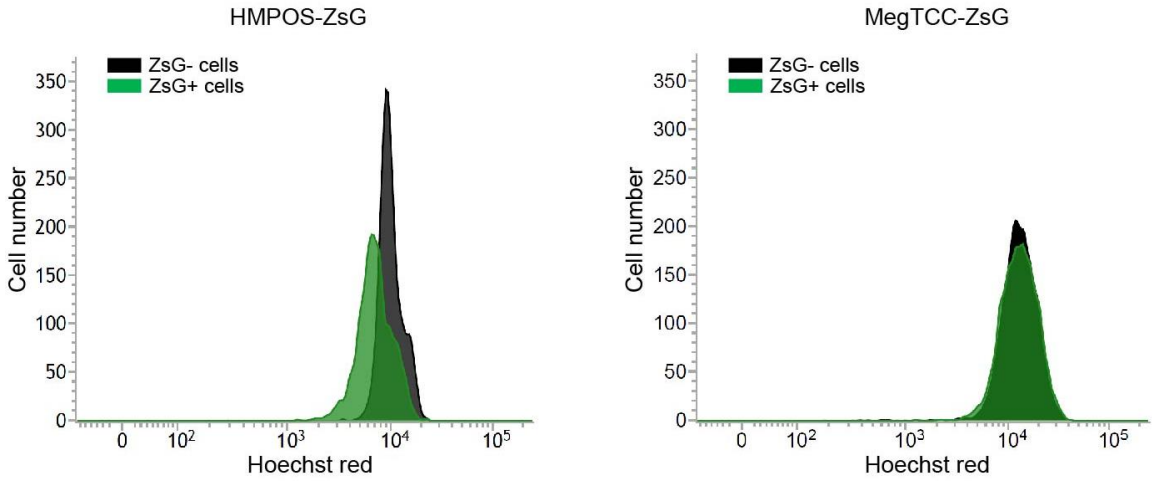

Figure I-7. Function of ABCG2 transporter

Efflux of Hoechst 33342 dye mediated by the function of ABCG2 transporter in HMPOS-ZsG and MegTCC-ZsG. The fluorescence intensity of Hoechst red is inversely related to the function of ABCG2 transporter.

A

Cell lines	Type of cells injected	No. of cells injected	Tumourigenesis	Tumour volume (mm^3)
HMPOS-ZsG	ZsG- cells	1×10^1	0/6 (0%)	-
	ZsG+ cells		4/6 (66.67%)	1,219.35 ± 1,175.20
	ZsG- cells	1×10^2	3/6 (50%)	496.83 ± 376.28
	ZsG+ cells		6/6 (100%)	1,376.76 ± 662.65
MegTCC-ZsG	ZsG- cells	1×10^3	0/6 (0%)	-
	ZsG+ cells		0/6 (0%)	-
	ZsG- cells	1×10^4	0/6 (0%)	-
	ZsG+ cells		2/6 (33.33%)	1,899.36 ± 412.19

B

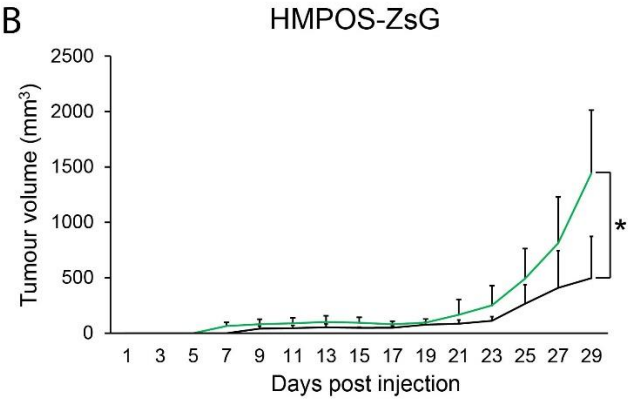

C

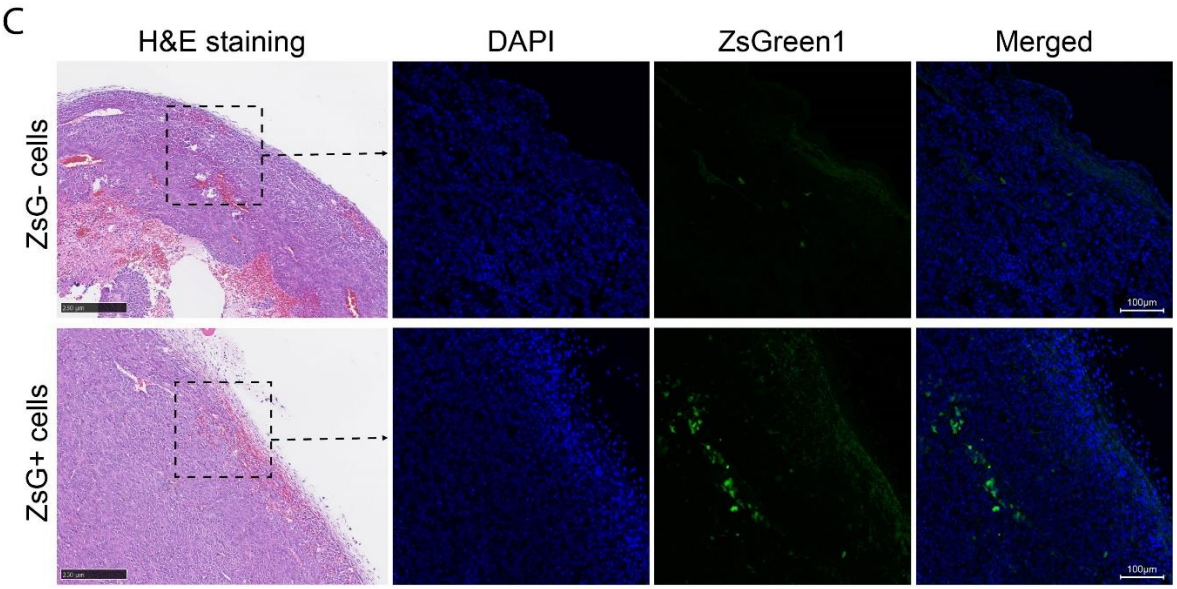

Figure I-8. Tumorigenic potential of ZsG+ cells in nude mice

(A) Tumorigenic potential of ZsG^+ cells with the data of No. of cells injected, tumorigenesis, and tumor volume. The data were presented with mean ± SD. (B) Comparison of the tumor growth between tumors derived from ZsG^- cells or ZsG^+ cells in HMPOS-ZsG. (C)

Histopathological comparison of the tumor sections derived from ZsG^- cells or ZsG^+ cells in HMPOS-ZsG. The tumor sections were stained with H&E or DAPI. Student's *t*-test was used for statistical analysis. $*p < 0.05$.

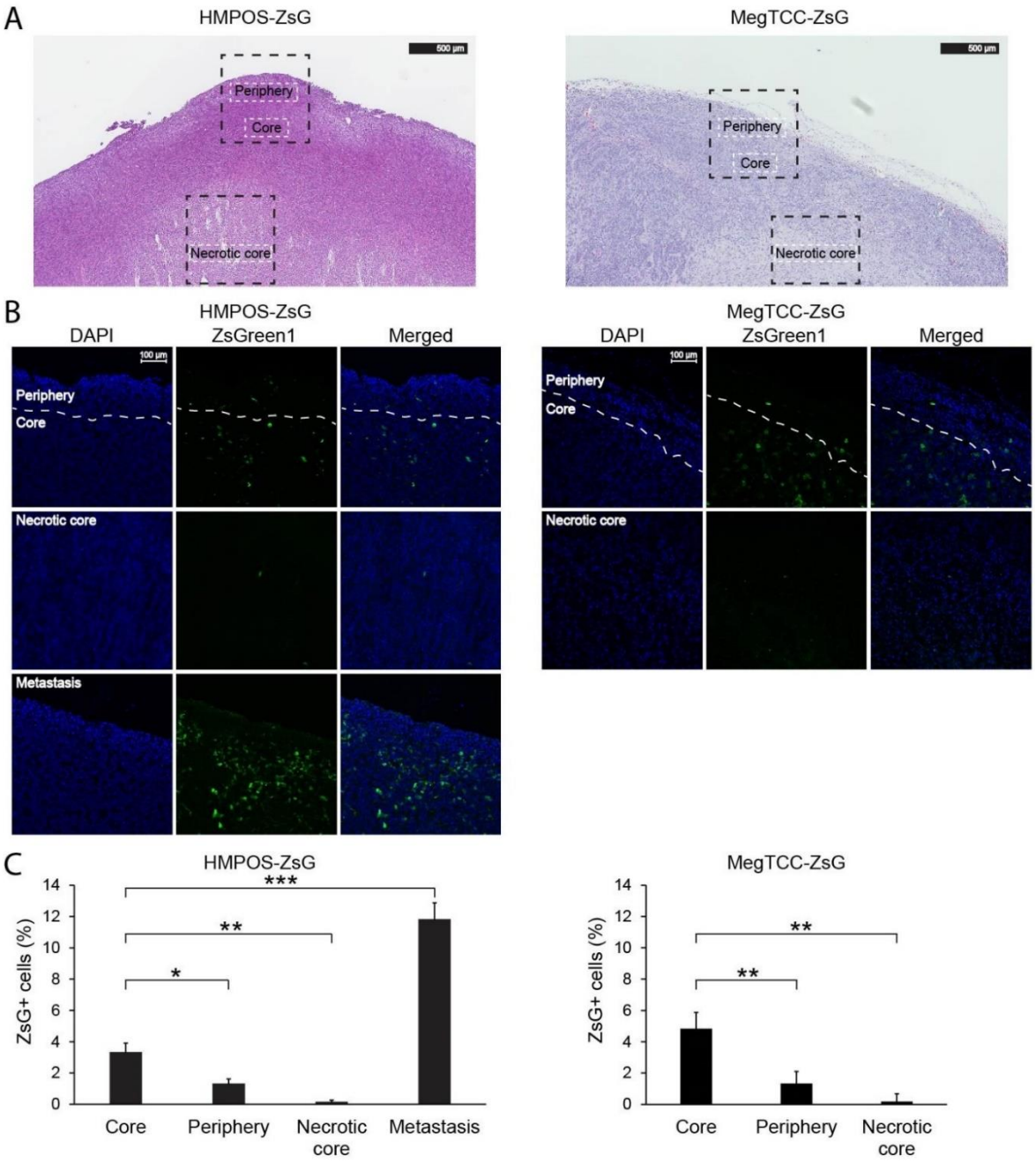

Figure I-9. Distribution of ZsG$^+$ cells in the different tumor regions in nude mice

(A) Histopathologically defined tumor regions using tumor sections which is stained with H&E. (B) Distribution of ZsG$^+$ cells in each tumor regions. Tumor sections stained with DAPI and fluorescence microscope were used for the evaluation. (C) Comparison of the ratio of ZsG$^+$ cells in each tumor regions including metastasis. Tukey's multiple comparison test was used for statistical analysis. *$p < 0.05$, **$p < 0.01$, and ***$p < 0.001$.

Table I-1. Primers for the cell line construction and selected cancer stem cell markers

Gene/Objective		Primer sequence	Product size (bp)
cODC1/PCR for CDS amplification	For	5'-GGG CCA ACA TGG CAA CTG ATT-3'	162
	Rev	5'-TGG CAC CTA CAC GTT AAT GCT-3'	
ZsGreen1/Sequencing	For	5'-GTG TAC AAG GCC AAG TCC GT-3'	106
	Rev	5'-CCA CTT CTG GTT CTT GGC GT-3'	
CD133	For	5'-ACC ATT GTG GTG CTC ACG TT-3'	156
	Rev	5'-CGG TTT GTT CAA CAC CAT GCC-3'	
CD200	For	5'-GGA GGA TGA AAT GCA GCC CT-3'	119
	Rev	5'-GGA GAC ACA CAG CCC TCA AC-3'	
KLF4	For	5'-TGC GTT ACT CGA CAA TGG CT-3'	131
	Rev	5'-GTA GTG CCT CGT CAG TTC GT-3'	
DPP4	For	5'-CAG TGG CTC CGA AGG ATT CA-3'	173
	Rev	5'-TAG AAG CTC TTC CCG TCG GA-3'	
CD44	For	5'-CCC CAT TAC CAA AGA CCA CGA-3'	140
	Rev	5'-GAG GTT TCC GCA TAG GAC CC-3'	
CD9	For	5'-CGG GAT TGC CGT AGT GAT GA-3'	123
	Rev	5'-TAG GGG TGG ACT TTC CTG CT-3'	
Thy1	For	5'-CGC TCC CGA ACC AAT TTC AC-3'	168
	Rev	5'-ACA CTT GAC CAG TTT GTC TCT GA-3'	
MCAM	For	5'-CCA TTG TGG CTG TGA CTG TGT-3'	193
	Rev	5'-TGT AGG AGG CCC ATC TCT TCT G-3'	

Table I-2. Conditions of conventional PCR reaction

Reaction		Condition	
PCR for *cODC1*	Pre-denaturation	94 °C, 2 min	
	Denaturation	98 °C, 10 s	35 cycles
	Annealing	51 °C, 30 s	
	Extension	68 °C, 30 s	
PCR for *ZsGreen1*	Pre-denaturation	94 °C, 5 min	
	Denaturation	94 °C, 30 s	35 cycles
	Annealing	58 °C, 30 s	
	Extension	72 °C, 30 s	

DISCUSSION

The identification and isolation of canine CSCs are challenging and the proteasome activity of CSCs in canine tumor cells remains unknown. Here, canine osteosarcoma cells, HMPOS, and canine transitional cell carcinoma cells, MegTCC, were visualized *via* their characteristics of low proteasome activity; the canine cancer cells were revealed to demonstrate CSC-like properties.

The CSC population was less than 3% among solid tumor cells [Ferletta *et al.*, 2011; He *et al.*, 2009; Pang *et al.*, 2014]. The small subpopulation of CSCs was resistant to conventional cancer therapies, which contributed to tumor recurrence [Chang, 2016]. Here, the visualized ZsG^+ cells also existed as a small population of adherent cells, consistent with previous results.

The ZsG^+ cell population after spheroid cell culture significantly increased compared with that in the adherent cell culture; ZsG^+ cells in a sphere could be observed visually. Moreover, the spheroid cells with enriched ZsG^+ cells exhibited low chymotrypsin-like-proteasome activity compared with the adherent cells, suggesting that canine CSCs can be identified by proteasome activity levels. Recently, the difference in the proteasome activities between the CSCs and non-CSCs was observed in human tumor cells [Voutsadakis, 2017]. Tumor cells with low proteasome activity exhibited CSC-like properties and resistance to tumor therapies in various human tumor cell lines [Lenos and Vermeulen, 2016]. Certain numbers of spheroid cells are CSC-enriched cells [Ma *et al.*, 2019; Shen *et al.*, 2015] exhibiting lower chymotrypsin-like-proteasome activity than adherent cells [Pan *et al.*, 2010; Vlashi *et al.*, 2009].

CSCs maintain their populations in tumors by orchestrating symmetric and asymmetric divisions related to self-renewal and differentiation capacity like the normal stem cells

[Morrison and Kimble, 2006; Bu *et al.*, 2013; Majumdar and Liu, 2020; Adikrisna *et al.*, 2012]. Time-lapse imaging revealed that the ZsG^+ cells had self-renewal and differentiation capacity through symmetric and asymmetric divisions; CSC visualization has enabled the real-time evaluation of this phenomenon in veterinary oncology [Tamari *et al*., 2014; Adikrisna *et al*., 2012; Hayashi *et al*., 2014]. Furthermore, the ratio of symmetric and asymmetric divisions indicated that the low ratio of the ZsG^+ cells was maintained similarly to that in the CSCs. Consistent with these results, the sorted ZsG^+ cells returned to their constant population size after 3 days of exhibiting differentiation capacity like the stem cells (Figure I-6) [Ayob and Ramasamy, 2018].

In the present study, the ZsG^+ cells had a small fraction of G0/G1 phase cells. According to previous studies, CSCs can be proliferative or dormant; they transition between the states following the tumor microenvironment [Tirino *et al*., 2008; Zhong *et al*., 2010; Chen *et al*., 2014]. *CD133*-expressing human osteosarcoma cells were highly proliferative and had tumorigenic capacity *in vitro* [Tirino *et al*., 2008]. Moreover, *CD133*-expressing human glioma cells were a small population of CSCs with proliferating characteristics *in vivo* [Lathia *et al*., 2011]. These results indicate that ZsG^+ cells would be proliferating CSCs and analysis of signalling pathways or gene expression related to cell cycle may enhance the understanding of the proliferation of ZsG^+ cells.

In this study, *CD133*, a reported CSC marker in canine tumor cells [Stoica *et al*., 2009; Deguchi *et al*., 2019; Michishita *et al*., 2011], was upregulated in the ZsG^+ cells in both the HMPOS-ZsG and MegTCC-ZsG. *CD133*, *KLF4*, *CD9*, *CD44, CD200* and *Thy1*, which are highly expressed in solid human tumors, could act as CSC markers [Singh *et al*., 2004; Collins *et al*., 2005; O'Brien *et al*., 2007; Prince *et al*., 2007; Jung *et al*., 2015; Wang *et al*., 2019; Shaikh *et al*., 2016]. As *CD133* is associated with the self-renewal capacity and tumorigenicity of CSCs [Stoica *et al*., 2009; Shi *et al*., 2011], it may be a good cell surface

marker for isolating CSCs from canine tumor cells. However, due to the *CD133* expression in differentiated cells [Karbanová *et al*., 2008; Feng *et al*., 2010] and the lack of cross-reactivity between canine antibodies and those of other species [Thamm *et al*., 2016; Deguchi *et al*., 2019; Rozemuller *et al*., 2010], it remains difficult to identify and isolate CSCs using CSC markers in canine tumor cells.

In the present study, the ZsG^+ cells were inefficiently stained by Hoechst 33342, indicating a higher function of the ABCG2 transporter than in the ZsG^- cells in the HMPOS-ZsG. However, in the MegTCC-ZsG, Hoechst 33342 staining did not reveal the function of the ABCG2 transporter in either the ZsG^- or ZsG^+ cells. ABC transporters play an important role in the chemoresistance and survival of CSCs [Begicevic and Falasca, 2017; Cho and Kim, 2020]. Although the chemoresistance of the ZsG^+ cells was not evaluated here, the ZsG^+ cells in the MegTCC-ZsG may express other subfamilies of ABC transporters, thus contributing to the chemoresistance of CSCs. For example, each of the subfamilies of ABC transporters, ABCB1, ABCB5 and ABCC1, were differentially produced in the CSCs in different types of tumor cells [Begicevic and Falasca, 2017; Cho and Kim, 2020].

In the present study, the ZsG^+ cells had a higher tumorigenic capacity than the ZsG^- cells after the sorting in the HMPOS-ZsG and MegTCC-ZsG cells. However, cell sorting might give light-induced damage to the cells [Stockley *et al*., 2017]. Also, cell sorting causes lesions in the mitochondrial DNA, thus decreasing mitochondrial membrane potential, increasing ROS and altering cell viability [Santos *et al*., 2003]. Here, the decreased plating efficiency and sphere-forming capacity after cell sorting (data not shown) was observed, indicating possible cell damage. Despite the damage caused by cell sorting, the sorted ZsG^+ cells exhibited a tumorigenic capacity similar to that in a previous study [Deguchi *et al*., 2019], where cell sorting was not performed for tumorigenic assay. Therefore, the visualization system here is still likely valid for CSC research.

In the present study, histopathological analyses were conducted to demonstrate that CSC visualization can be used to trace CSCs *in vivo* and revealed that the tumors formed by the ZsG^+ cells had widely distributed ZsG^+ cells in a larger volume than that of the tumors formed by the ZsG^- cells. These results indicate that the ZsG^+ cells should be proliferative. The cells in a tumor proliferate at varying rates, depending on the histopathological regions. The cells inside a tumor tend to proliferate slowly with a low mitotic index and low level of Ki67, a marker for cell proliferation [Wang *et al*., 2015; Gil *et al*., 2013; Yi *et al*., 2019]. Contrarily, the cells in the metastatic region exhibit highly proliferative characteristics [Wang *et al*., 2015; Lee *et al*., 2012]. Tumor cell proliferation may involve tumor vascularity. The blood vessels in the tumors play important roles in providing oxygen and energy to tumor cells and the route for metastasis [Schaaf *et al*., 2018; Weis and Cheresh, 2011]. Low vascularity is related to the necrosis and low proliferation of tumor cells [Urnauer *et al*., 2017; Zaidi *et al*., 2019; Linkous *et al*., 2010]. Here, the ZsG^+ cells were broadly distributed in the proliferative tumor regions, especially the metastatic region, suggesting that the ZsG^+ cells are proliferative and the proliferation might be related to tumor oxygenation and energy metabolism.

During the identification of therapeutic targets of canine CSCs, a visualization system, as a research tool, will support the formulation of new strategies to eradicate CSCs. For the first time, canine tumor cells with low proteasome activity and CSC-like properties can be visualized. In the future, it will be necessary to assess the metabolism and therapeutic resistance of ZsG^+ cells using the visualization system to target CSCs.

SUMMARY

CSCs are recognized as a cause of treatment failure in various tumors. However, establishing CSC-targeted therapies has been hampered by difficulties in identification and isolation of this small subpopulation of cells. Recent studies have revealed that tumor cells with low proteasome activity have a CSC phenotype that can be utilized for canine CSCs visualization. The purpose of this study was to visualize CSCs in two canine cell lines, HMPOS and MegTCC. The parent cells were genetically engineered to express the ZsGreen1 fluorescent protein connected to the carboxyl-terminal degron of canine ornithine decarboxylase that was accumulated along the low proteasome activity, ZsG^+ cells. A few ZsG^+ cells were observed, and the mode of action of this system was confirmed by using proteasome inhibitor (MG-132), increasing the fluorescence intensity of ZsGreen1. The CSC-like properties of ZsG^+ cells were evaluated on cell divisions, cell cycle, expression of CSC markers and tumorigenicity. ZsG^+ cells underwent asymmetric divisions and had a low percentage of G0/G1 phase cells. Moreover, ZsG^+ cells expressed CSC markers such as *CD133* and showed tumorigenic capacity with large volume of tumors. In histopathological analysis, ZsG^+ cells widely distributed in the tumor sections derived from ZsG^+ cells and the proliferative regions of the tumors. The results of this study indicate visualized canine tumor cells with low proteasome activity have a CSC-like phenotype, and this visualization system can be utilized to identify and isolate the canine CSCs.

CHAPTER II

Sulfasalazine radiosensitizes canine tumor cells with low proteasome activity through depleting glutathione and enhancing DNA damage by X-irradiation

INTRODUCTION

CSCs or tumor-initiating cells are a distinct subpopulation with particular surface markers which possesses unlimited cell growth, metastatic capability undergoing self-renewal, asymmetric cell division, and differentiation [Walcher *et al*., 2020]. Difference of radiosensitivity is explained by the tumor heterogeneity which is in charge of the reason that tumor cells are affected by radiation therapy inconsistently [Olivares-Urbano *et al*., 2020]. Radio-resistance of tumor cells, especially CSCs, make it difficult to eradicate tumor cells completely suggesting that understanding of the radio-resistance mechanism is essential [Li *et al*., 2021; Arnold *et al*., 2020].

CSC visualization system was constructed for isolation and identification of CSCs as previously described in the first chapter. In this system, canine tumor cells were engineered to express a ZsGreen1 fluorescent protein which is connected to a proteasome degron, and canine CSCs were visualized owing to their property of low proteasome activity, ZsG^+ cells. Finally, the ZsG^+ cells which could exhibit CSC-like properties were successfully isolated using a flow cytometric cell sorter.

Various factors influencing the radio-resistance of CSCs include degree of DNA damage, DNA ploidy, respiratory metabolism, production of ROS, GSH, and so on [Arnold *et al*., 2020; Rycaj and Tang, 2014; Lyakhovich and Lleonart, 2016]. p53-binding protein 1 (53BP1) is an important component of DNA-double strand break (DSB) signaling and mediates the non-homologous end-joining-mediated DSB repair. 53BP1 is employed as a marker for DNA damage and repair [Sekhar *et al*., 2019; Shimamura *et al*., 2018; Marková *et al*., 2007]. DNA ploidy of tumors are implicated as a prognostic factor of tumors [Pradhan *et al*., 2012; Yang *et al*., 2020; Syrios *et al*., 2013], and aneuploidy is related to radio-resistance of tumor cells

[Walter *et al*., 1991; Schwartz *et al*., 1999]. In addition, respiratory metabolism is also an important factor contributing to radio-resistance of tumor cells [McCann *et al*., 2021]. Research on energy metabolism of CSCs often reports low mitochondrial respiration of CSCs and relatively up-regulated glycolysis of CSCs [Palorini *et al*., 2014; Sun *et al*., 2017]. However, recent reports suggest metabolic plasticity of CSCs between mitochondrial respiration and glycolysis, which is regulated by the interaction of CSCs and tumor microenvironment [Walsh *et al*., 2019; Snyder *et al*., 2018].

In radiation therapy, generation of ROS plays a role of indirect damage to tumor cells, and this is a major effect of low-LET radiation such as X-ray and gamma ray [Desouky et al., 2015; Kawamura *et al*., 2018]. Therefore, the ROS is a key factor to solve the radio-resistance of tumor cells [Wang *et al*., 2019]. To counteract the production of ROS after irradiation, CSCs have increased contents of reductants such as GSH indicating that reductants can be effective targets of CSCs in radiation therapy [Diehn *et al*., 2009; Rycaj and Tang, 2014]. A cystine/glutamate antiporter which is called xCT or SLC7A11 is involved in the biosynthesis of GSH and maintains redox balance of tumor cells [Lim *et al*., 2019]. Inhibition of xCT using sulfasalazine which is used for inflammatory bowel disease in dogs disrupts the redox balance of human tumor cells [Nagane *et al*., 2018; Cobler *et al*., 2018]. The inhibition of xCT using sulfasalazine induces tumor cell death via ferroptosis and apoptosis through GSH deprivation [Koppula *et al*., 2021]. In addition, sulfasalazine targets CSCs having high expression level of CSC marker like CD133 or CD44v [Song *et al*., 2017; Thanee *et al*., 2021], and sulfasalazine prolongs survival of rat brain tumor models by inducing CSCs death [Haryu *et al*., 2018]. In a clinical study where sulfasalazine was used for treatment of gastric tumor patients, sulfasalazine still shows the effect of reducing a population of CSCs in gastric tumor tissues [Shitara *et al*., 2017]. In the first chapter, visualized canine CSCs exhibited up-regulated *CD133* indicating that sulfasalazine may

target canine CSCs. Therefore, sulfasalazine would be a promising candidate to radiosensitize canine CSCs.

Tumor cells with low proteasome activity preserve cancer stem-like properties including radio-resistance [Munakata *et al*., 2016; Della Donna *et al*., 2012] in which CSCs related proteins are stabilized by the characteristic of low proteasome activity [Chen *et al*., 2005; Deng *et al*., 2020]. However, the radiosensitivity of canine tumor cells with low proteasome activity and the mechanism are not clear, even in human tumors.

Thus, in the present study, the radio-resistance and its mechanism of canine tumor cells with low proteasome activity were explored investigating radio-resistance, degree of DNA damage after X-irradiation, DNA ploidy, respiratory metabolism, production of ROS after X-irradiation, GSH contents. Then, xCT was investigated using sulfasalazine as a target for canine CSCs in radiation therapy.

MATERIALS AND METHODS

Cell culture condition

In the first chapter, canine cell lines HMPOS and MegTCC were engineered to express ZsGreen1-cODC, generating HMPOS-ZsG and MegTCC-ZsG. Subsequently, HMPOS-ZsG and MegTCC-ZsG were used in this study. All tumor cells were cultured in RPMI-1640 media (Gibco) supplemented with 10% FBS (Sigma-Aldrich), 100 units/mL penicillin G, 100 μg/mL streptomycin (Wako), and 10 μg/mL blasticidin (Wako) in a humidified incubator at 37°C and 5% CO_2.

Flow cytometry and cell sorting

HMPOS-ZsG and MegTCC-ZsG cells were washed with PBS and suspended using 0.025% trypsin-EDTA for subsequent FACS analysis using a FACSVerse flow cytometer (BD Biosciences) or cell sorting using a FACSAria II flow cytometer (BD Biosciences). Based on fluorescence intensity of ZsGreen1, ZsG^- and ZsG^+ cells were defined as described in the first chapter.

Irradiation

Cultured tumor cells were irradiated with x-rays using a Titan 320s X-ray generator (Shimadzu Corporation, Kyoto, Japan) at room temperature (dose rate 4.62 Gy/min, 200 kVp, 20 mA with a 1.5 mm aluminum filter).

Clonogenic survival assay

The sorted ZsG^- and ZsG^+ cells were plated on 60 mm cell culture dishes, respectively

and incubated for 6 or 12 hours. Then, the cells were x-ray irradiated followed by changing cell culture media to new media and were allowed to form colonies for 6 or 7 days at 37°C and 5% CO_2. Methanol fixation and staining of the colonies were performed using Giemsa solution (Wako), and colonies containing over 50 cells were counted using Image J software (National Institutes of Health, Bethesda, MD, USA). Plating efficiency (PE) was calculated and used to normalize every survival fraction.

Immunofluorescence microscopy

The immunofluorescence microscopy was performed as previously described [Deguchi *et al*., 2019] with some modification. Briefly, cancer cells were plated on glass cover slips and incubated. Then, the cells were irradiated with 1 Gy X-ray and incubated with different time courses for each group. The cells were fixed using 4% paraformaldehyde (Wako) and permeabilized using PBS containing 0.5% Triton X-100. After washing with PBS and incubation with blocking buffer, the cells were stained with a primary antibody rabbit anti-53BP1 (1:2,000; Abcam Inc., Cambridge, UK) and a secondary antibody goat anti-rabbit Alexa Fluor 555 (1:2,000; Invitrogen). At the end of the experiment, the cells were counterstained with NucBlue (Invitrogen) according to the manufacturer's instruction and mounted with ProLong Diamond Antifade Mountant (Invitrogen) for fluorescence microscopic analysis under an Olympus BX50 microscope (Olympus, Tokyo, Japan). Number of 53BP1 foci which were appeared as fluorescent dots.

DNA ploidy analysis

DNA contents was measured for the DNA ploidy analysis. First of all, tumor cells were seeded at 1×10^5 cells in a 10 cm dish and incubated for 3 days. After washing the cells using PBS, the cells were dissociated into single cells by trypsinization. Then, the cells were

centrifuged at 300 × g for 5 minutes at 4°C and fixed with 500 μL of cold 2% paraformaldehyde (Wako) for 1 hour at 4°C. After centrifugation at 300 × g for 5 minutes at 4°C, the cells were washed with cold PBS. Membrane permeabilization was performed by incubating the cells at 4°C for 4 hours in 1 mL of 70% ethanol which was prepared at −20°C previously. Subsequently, the cells were washed with cold PBS after centrifugation at 300 × g for 5 minutes at 4°C, and then the cells were incubated in 1 mL of 40 μg/mL propidium iodide (Sigma-Aldrich) with 100 μg/mL of ribonuclease A for 30 minutes in a 37°C water bath under dark condition. DNA contents were measured using a FACSVerse flow cytometer (BD Biosciences), and DNA ploidy of the cells was evaluated. Based on DNA index (DI), DNA ploidy was determined following previous studies [Gauwitz et al., 1994; Pradhan et al., 2012].

Cell mito stress test

The sorted ZsG^- cell and ZsG^+ cells were plated in 8 well XFp cell culture miniplates (Seahorse Bioscience, North Billerica, MA, USA) at a density of 3×10^4 cells/well and incubated for 6 or 12 hours at 37°C and 5% CO_2. Then, the cells were washed 3 times with Seahorse XF RPMI medium which is supplemented with 300 mg/L glutamine and 2,000 mg/L glucose and were incubated in 180 μL of the same medium for 1 hour at 37°C and non-CO_2. Working concentration of oligomycin, carbonyl cyanide 4-(trifluoromethoxy)phenylhydrazone (FCCP) and rotenone/antimycin A was adjusted to 1.5 μM, 0.5 μM and 0.5 μM, respectively. Subsequently, oxygen consumption rate (OCR) was measured using a Seahorse XFp Analyzer (Seahorse Bioscience) according to the manufacturer's protocol. During measurement of OCR, injection of oligomycin (ATP synthase inhibitor) decreases mean OCR of cells and shows ATP-linked respiration. Addition of FCCP (potent uncoupler of oxidative phosphorylation) increases mean OCR of cells

showing maximal respiratory capacity, and injection of rotenone/antimycin A (electron transport inhibitor) decreases mean OCR of cells providing information about proton leak and non-mitochondrial respiration.

Reactive oxygen production detection

Accumulation of ROS was measured using CellROX® Deep Red Reagent (Life Technologies, Carlsbad, CA, USA) according to the manufacturer's protocol. Cells were plated on 60 mm cell culture dishes and incubated for 3 days at 37°C and 5% CO_2, followed by X-ray irradiation with 5 Gy. At 24 hours after irradiation, CellROX® Deep Red Reagent (Life Technologies) was added to the cells (final concentration, 5 μM) and the cells were incubated for 30 minutes at 37°C and 5% CO_2. Then, the cells were washed three times with PBS and resuspended for analysis using FACSVerse flow cytometer (BD Biosciences).

Glutathione assay

Glutathione content was measured using a GSH-Glo™ Glutathione Assay (Promega) as described by the manufacturer. Briefly, the sorted ZsG^- and ZsG^+ cells were plated at 5×10^3 cells/well in 96-white well plates (Greiner Bio-One, Frickenhausen, Germany), and the cells incubated for 6 or 12 hours at 37°C and 5% CO_2. After removing the culture medium, the cells were incubated with 100-μL GSH-Glo™ Reagent for 30 minutes at room temperature. At 15 minutes after addition of 100-μL reconstituted Luciferin Detection Reagent, the luminescence intensity was measured using a microplate reader (Infinite 200, Tecan Japan).

Protein sample preparation and Western blot analysis

For Western blot analysis, rabbit anti-SLC7A11 polyclonal antibody (Catalog # MBS3207121) was purchased from MyBioSource (San Diego, CA, USA). Rabbit anti-β-

actin monoclonal antibody (Catalog # 4970) and HRP conjugated anti-rabbit IgG (Catalog # 7074) were purchased from Cell Signaling Technology (Danvers, MA, USA).

ZsG^- cells, ZsG^+ cells, and adherent cells cultured with 0.5- or 1-μM MG-132 for 12 hours were prepared in the HMPOS-ZsG. Total protein extraction was performed through the process of cell lysis using ice-cold sample buffer [62.5 mM Tris-HCl (pH 6.8), 2.5% sodium dodecyl sulfate (SDS), 10% glycerol, 5% β-mercaptoethanol, 0.002% bromophenol blue], sonification for 15 seconds. Then, the concentration of protein extracts was measured using a protein quantification assay (Macherey-Nagel, Dürren, Germany) according to the manufacturer's instruction. The protein extracts (5 μg) were separated on 4–12% gradient SDS–poly-acrylamide gel electrophoresis (PAGE) and blotted on to polyvinylidene difluoride (PVDF) membrane. Subsequently, the membranes were blocked with PBS containing 0.05% tween 20 (PBST) supplemented with 3% bovine serum albumin (BSA) for 1 hour at room temperature. After washing with PBST three times, the membranes were incubated with the anti-SLC7A11 antibody (1:2,000) or anti-β-actin antibody (1:3,000) in PBST with 1% BSA overnight at 4℃. The membranes were washed three times and incubated with the HRP conjugated anti-rabbit IgG (1:10,000) for 1 hour at room temperature. Following incubation with Western Blot Ultra-Sensitive HRP substrate (TaKaRa), the chemiluminescent signals from protein-antibody complexes were obtained using Image Quant LAS 4000 mini (Fujifilm, Tokyo, Japan). The intensity of bands was quantified using Image J software (National Institutes of Health) and normalized by β-actin band intensity.

Statistical analysis

Results are presented as mean ± SD. Statistical analysis was conducted using IBM SPSS Statistics version 26.0 (IBM). Normality of the results were evaluated using Shapiro–Wilk test. Statistical significance between groups was determined using one-way ANOVA followed

by Tukey's multiple comparison test. A *p*-value less than 0.05 (*p), 0.01 (**p) or 0.001 (***p) was considered statistically significant.

RESULTS

Ratio of ZsG$^+$ cells after irradiation

The HMPOS-ZsG and MegTCC-ZsG expressing ZsGreen1-cODC were established in the first chapter, and tumor cells with low proteasome activity were green fluorescent cells possessing CSC-like properties (ZsG$^+$ cells). In this study, the ratio of ZsG$^+$ cells was evaluated using confocal microscopy and flow cytometry after irradiation with different radiation doses. The ratio of ZsG$^+$ cells increased radiation dose-dependently (Figure II-1A-B) at 3 days after irradiation in both HMPOS-ZsG and MegTCC-ZsG. In addition, the ratio of ZsG$^+$ cells increased time-dependently after 7.5 Gy irradiation in HMPOS-ZsG (Figure II-2A-B).

Radio-resistance of ZsG$^+$ cells

To evaluate radio-resistance of the cells, clonogenic assay was performed with irradiation using sorted ZsG$^-$ and ZsG$^+$ cells. After 6 or 12 hours of cell sorting, X-irradiation was performed since the ratio of ZsG$^+$ cells decreases after cell sorting as described previously. When the cells were irradiated at 6 hours after cell sorting, the ZsG+ cells exhibited higher survival fraction than the ZsG$^-$ cells at 2 and 5 Gy in both HMPOS-ZsG (2 Gy, 0.62 ± 0.02 and 0.79 ± 0.00, p = 0.015; 5 Gy, 0.25 ± 0.06 and 0.44 ± 0.01, p = 0.008 for the ZsG$^-$ and ZsG$^+$ cells, respectively) and MegTCC-ZsG (2 Gy, 0.45 ± 0.03 and 0.73 ± 0.04, p = 0.000; 5 Gy, 0.05 ± 0.00 and 0.15 ± 0.00, p = 0.023 for the ZsG$^-$ and ZsG$^+$ cells, respectively) (Figure II-3A). When the cells were irradiated at 12 hours after cell sorting, the ZsG$^+$ cells exhibited higher survival fraction than the ZsG$^-$ cells at 5 Gy in HMPOS-ZsG (0.27 ± 0.01 and 0.43 ± 0.01, p = 0.045 for the ZsG$^-$ and ZsG$^+$ cells, respectively) and at 2 and 5 Gy in MegTCC-ZsG

(2 Gy, 0.54 ± 0.02 and 0.79 ± 0.06, p = 0.001; 5 Gy, 0.09 ± 0.02 and 0.23 ± 0.00, p = 0.022 for the ZsG^- and ZsG^+ cells, respectively) (Figure II-3B).

Accumulation of 53BP1 foci in ZsG^+ cells after X-irradiation

Different levels of DSB were confirmed by evaluating the accumulation of 53BP1 foci formation after X-irradiation in ZsG^- and ZsG^+ cells. Background levels of 53BP1 foci per nucleus was less than 5 in all groups. After 0.5 hours of X-irradiation, the lower number of 53BP1 foci was presented in ZsG^+ cells than that of ZsG^- cells in both HMPOS-ZsG (12.80 ± 5.61 and 19.12 ± 3.99 for the ZsG^- and ZsG^+ cells, respectively, p = 0.000) and MegTCC-ZsG (14.80 ± 3.01 and 20.12 ± 2.96 for the ZsG^- and ZsG^+ cells, respectively, p = 0.000). After 1 hour of X-irradiation, the lower number of 53BP1 foci was presented in ZsG^+ cells than that of ZsG^- cells in MegTCC-ZsG (9.88 ± 2.57 and 13.36 ± 2.12 for the ZsG^- and ZsG^+ cells, respectively, p = 0.000) (Figure II-4A-B).

Nuclear DNA ploidy of the cells

Patterns of the nuclear DNA ploidy was evaluated in ZsG^- and ZsG^+ cells. The distinct peak of G0/G1 was regarded as DI of 1 and another distinct peak of G2/M was regarded as DI of 2. The tumor cells showed diploid G0/G1 and diploid G2/M peaks in the DNA histogram in both ZsG^- and ZsG^+ cells. However, non-diploid peak was not detected (Figure II-5A-B).

Mitochondrial function of ZsG^+ cells

There was no significant difference of OCR between ZsG^- and ZsG^+ cells in basal respiration, maximal respiration, proton leak, ATP-linked respiration and spare respiratory capacity in HMPOS-ZsG after 6 or 12 hours-incubation and MegTCC-ZsG after 6-hours incubation. However, in MegTCC-ZsG after 12 hours-incubation, ZsG^+ cells exhibited higher OCR than ZsG^- cells in basal respiration ($p = 0.027$), maximal respiration ($p = 0.016$), ATP-linked respiration ($p = 0.028$) and spare respiratory capacity ($p = 0.015$) (Figure II-6A-B).

Level of ROS in ZsG^+ cells after X-irradiation

Cellular ROS level was assessed using CellROX® Deep Red staining after X-irradiation. The CellROX fluorescence intensity of ZsG^+ cells were lower than that of ZsG^- cells in HMPOS-ZsG and MegTCC-ZsG after X-irradiation (Figure II-7A). In addition, the results are presented in Figure II-7B with relative values, and the relative CellROX fluorescence intensity in ZsG+ cells was significantly lower than that in ZsG^- cells after X-irradiation in HMPOS-ZsG ($p = 0.040$) and MegTCC-ZsG ($p = 0.025$) (Figure II-7B).

GSH content in ZsG^+ cells

Following the evaluation of cellular ROS level, total GSH content was measured in ZsG^- and ZsG^+ cells. The total GSH content was significantly lower in ZsG^- cells compared with ZsG^+ cells in HMPOS-ZsG (6 hours, $p = 0.000$; 12 hours, $p = 0.003$) and MegTCC-ZsG (6 hours, $p = 0.002$; 12 hours, $p = 0.001$) (Figure II-8).

Protein level of xCT at low proteasome activity

The results of Western blot analysis demonstrated a relationship between xCT and proteasome activity. The protein expression of xCT in ZsG^- cells was markedly lower than that in ZsG^+ cells which exhibited low proteasome activity in the first chapter. In addition, the expression of xCT in adherent cells increased after treatment with MG-132 in a dose-dependent manner (Figure II-9).

Role of xCT in the radio-resistance of ZsG^+ cells

Next, sulfasalazine was employed to inhibit the activity of xCT in the HMPOS-ZsG cells. In the GSH contents analysis, sulfasalazine dose-dependent decrease of GSH contents was observed in both the ZsG^- and ZsG^+ cells. After adding 500-μM or higher concentrations of sulfasalazine to the cells for 6 hours, differences of GSH contents between the ZsG^- and ZsG^+ cells were disappeared. After adding 1,000-μM or 1,500-μM sulfasalazine to the cells for 12 hours, differences of GSH contents between the ZsG^- and ZsG^+ cells were disappeared. Dose-dependent decrease of GSH contents was also observed in the ZsG^- and ZsG^+ cells along with the dose increase of xCT (Figure II-10A).

Cellular ROS level was measured after incubation with 1,000-μM sulfasalazine for 6 or 12 hours with or without X-irradiation. In the control (Con) and sulfasalazine (Sulfa) groups, there was no difference of CellROX fluorescence intensity between ZsG^- and ZsG^+ cells, but after X-irradiation, ZsG^+ cells exhibited lower CellROX fluorescence intensity than ZsG^- cells did (6 hours incubation with sulfasalazine, $p = 0.000$; 12 hours incubation with sulfasalazine, $p = 0.018$). The difference between ZsG^- and ZsG^+ cells after X-irradiation disappeared when the cells were incubated with sulfasalazine (Figure II-10B).

The results of 53BP1 immunofluorescence staining showed that xCT inhibition by 1,000-μM sulfasalazine increases DSB not only in the ZsG^- cells, but also in ZsG^+ cells. However,

the effects of xCT inhibition in the initial DSB was more significant in the ZsG^+ cells than in ZsG^- cells (Figure II-10C).

Radiosensitizing effects of sulfasalazine was evaluate using clonogenic survival assay. In the ZsG^- cells, the suppression of xCT by 1,000-μM sulfasalazine exhibited tendency of radiosensitization, but there was no significant difference. However, the suppression of xCT by 1,000-μM sulfasalazine significantly radiosensitized ZsG^+ cells at 2 ($p = 0.014$) and 5 Gy ($p = 0.016$) after 6 hours incubation with sulfasalazine and at 5 Gy ($p = 0.040$) after 12 hours incubation with sulfasalazine (Figure II-10D).

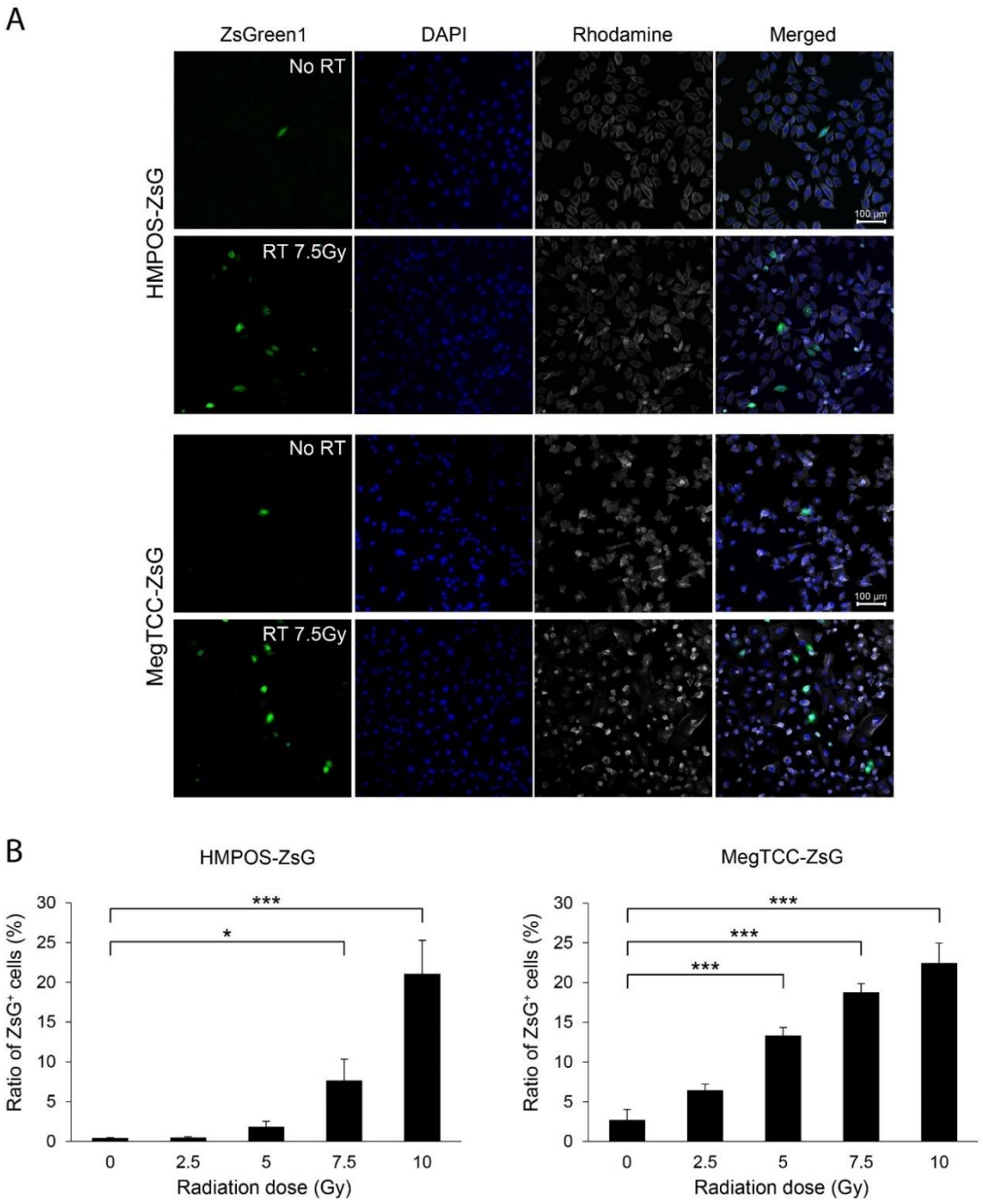

Figure II-1. Ratio of ZsG$^+$ cells after exposure to X-irradiation

(A) Fluorescence images of HMPOS-ZsG and MegTCC-ZsG cells showing change of the ratio of ZsG+ cells after exposure to X-irradiation. (B) Dose-dependent change of the ratio of ZsG$^+$ cells after X-irradiation in HMPOS-ZsG and MegTCC-ZsG. The data were presented with mean ± standard deviation. Tukey's multiple comparison test was used for statistical analysis. *$p < 0.05$ and ***$p < 0.001$.

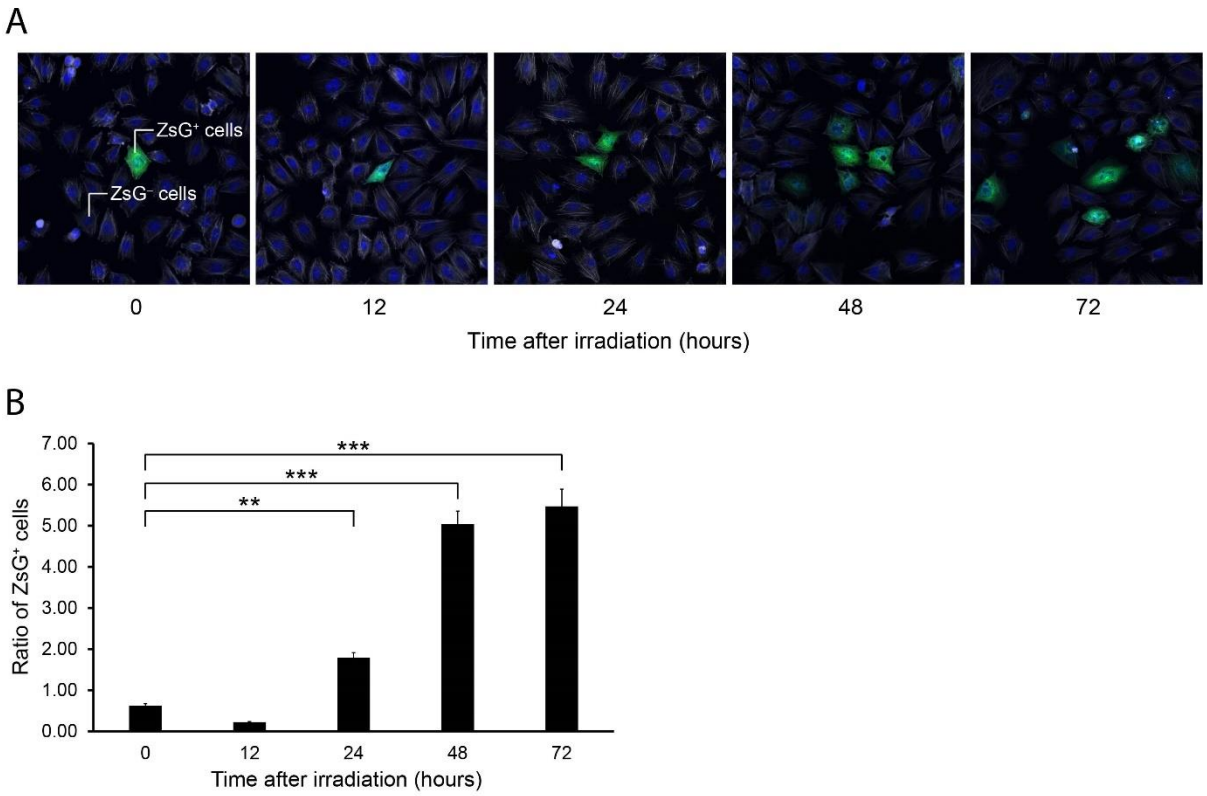

Figure II-2. Ratio of ZsG^+ cells following times after X-irradiation

(A) Confocal microscopic images showing time-dependent change of a ZsG^+ cell ratio after X-irradiation in HMPOS-ZsG. (B) Result of flow cytometric analysis indicating time-dependent change of the ratio of ZsG^+ cells after X-irradiation in HMPOS-ZsG. The data were presented with mean ± standard deviation. Tukey's multiple comparison test was used for statistical analysis. $^{**}p < 0.01$ and $^{***}p < 0.001$.

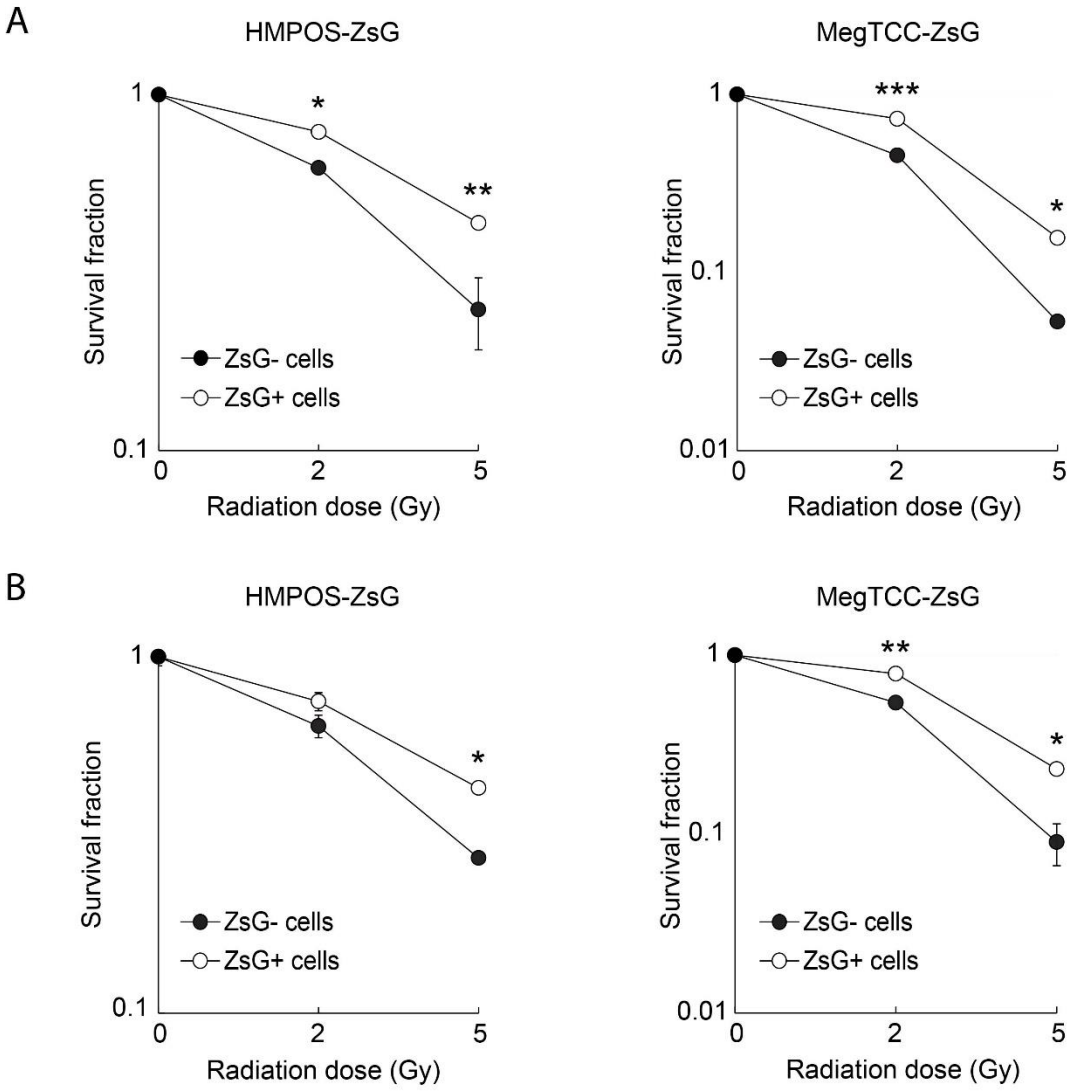

Figure II-3. Radio-resistance of ZsG$^+$ cells

Radiation survival curves of the ZsG$^-$ and ZsG$^+$ cells, which were evaluated using clonogenic survival assay at 6 hours of incubation (A) or 12 hours of incubation (B) after cell sorting. The data were presented with mean ± standard deviation. Tukey's multiple comparison test was used for statistical analysis. *$p < 0.05$, **$p < 0.01$, and ***$p < 0.001$.

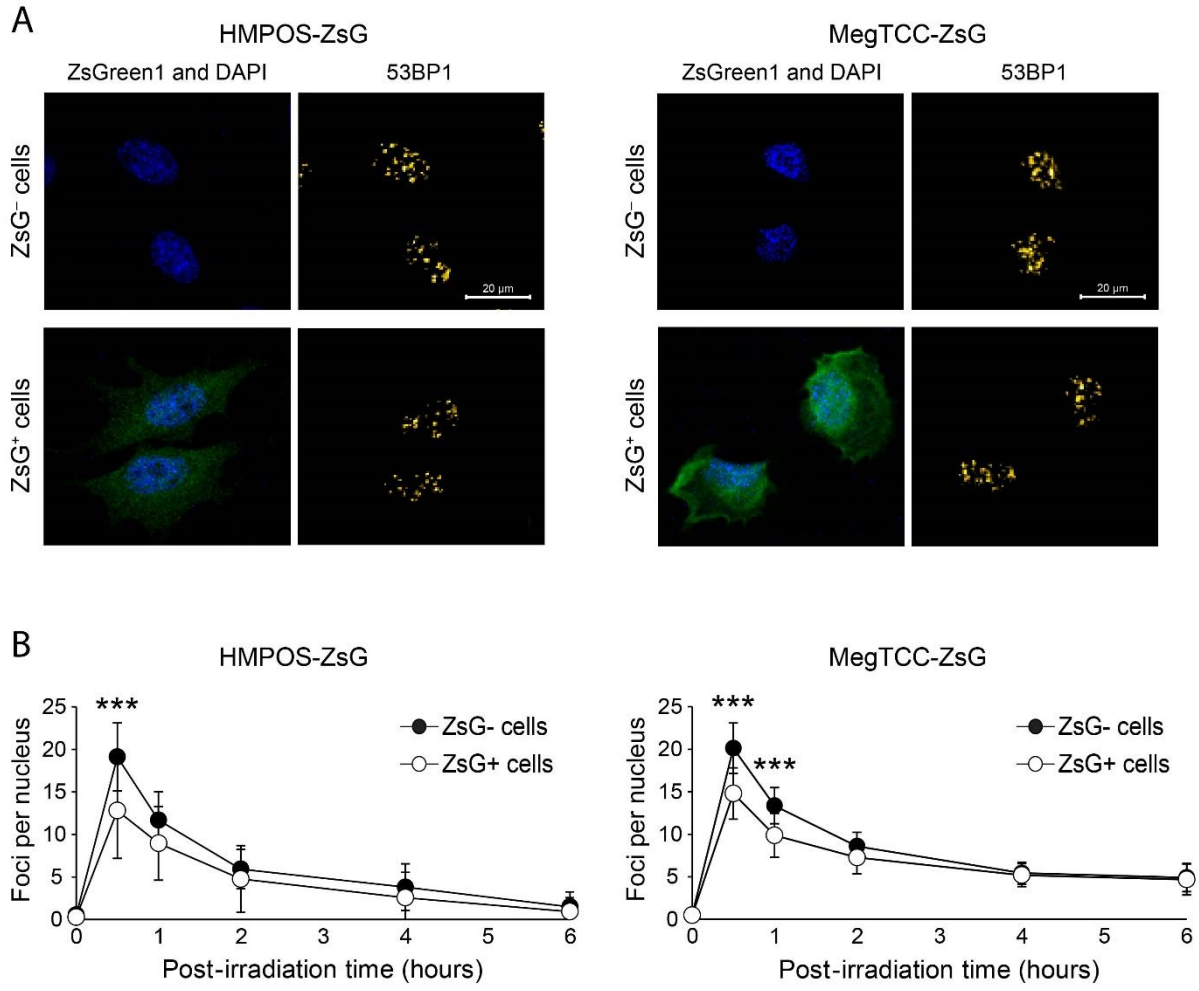

Figure II-4. Accumulation of 53BP1 foci in ZsG$^+$ cells after X-irradiation

(A) Fluorescence images of ZsGreen1, DAPI, and 53BP1 in ZsG$^-$ and ZsG$^+$ cells after 0.5 hours of X-irradiation with 1 Gy. (B) Time-dependent changes of the average number of 53BP1 foci in ZsG$^-$ and ZsG$^+$ cells after X-irradiation with 1 Gy. The data were presented with mean ± standard deviation. Tukey's multiple comparison test was used for statistical analysis. ***$p < 0.001$.

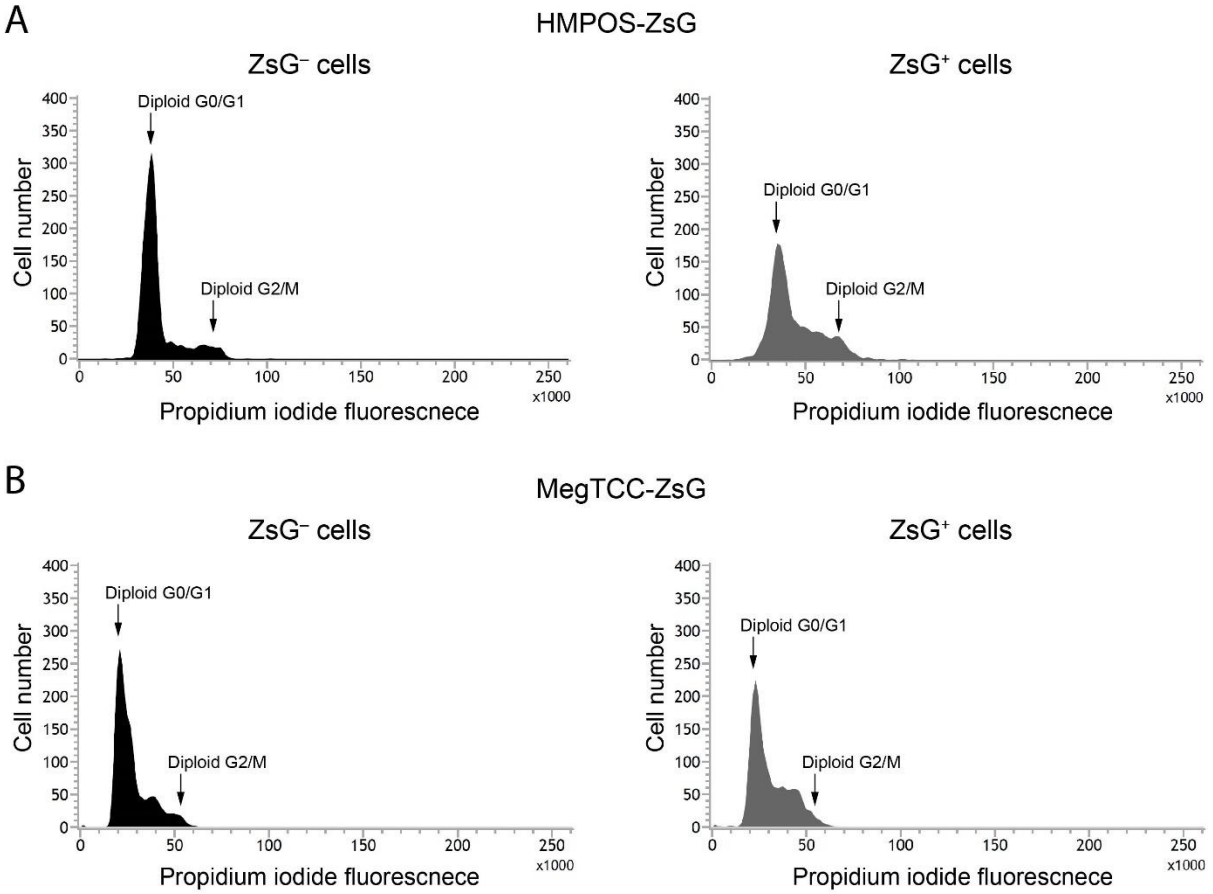

Figure II-5. Nuclear DNA ploidy of the cells

Flow cytometric histogram showing DNA contents of the tumor cells in HMPOS-ZsG (A) and MegTCC-ZsG (B). Two peaks of diploid G0/G1 and diploid G2/M indicates diploid DNA. Non-diploid peak was not observed.

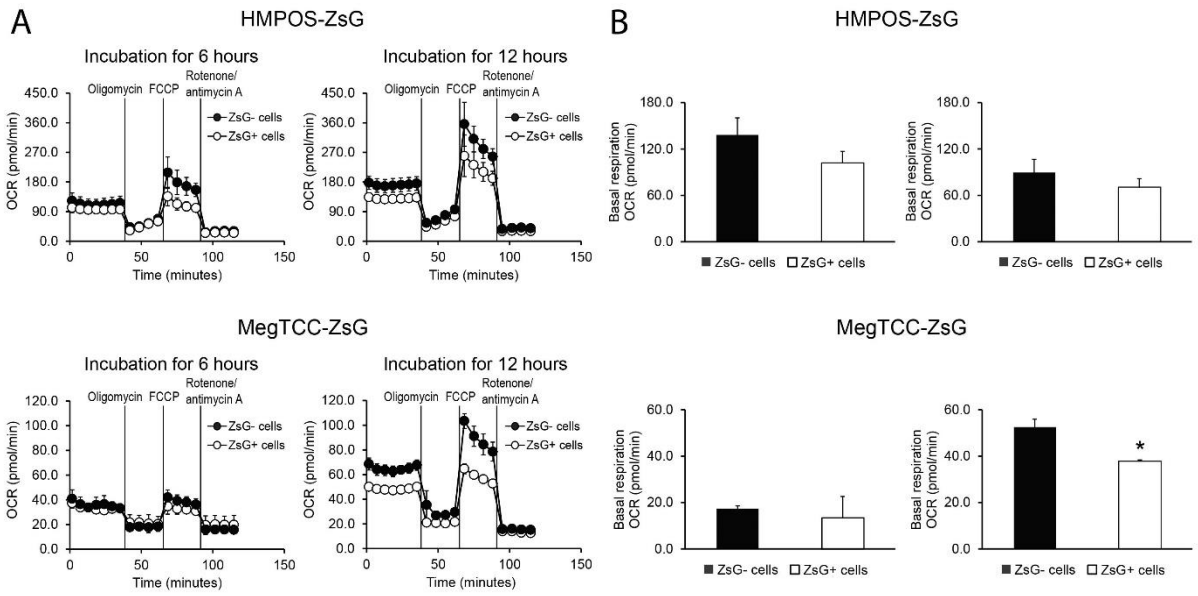

Figure II-6. Mitochondrial function of ZsG$^+$ cells

(A) Measurements of oxygen consumption rate (OCR) showing mitochondrial function of ZsG$^-$ and Zsg$^+$ cells in HMPOS-ZsG and MegTCC-ZsG. (B) Bar graphs indicating basal respiration of the cells, which were calculated from the results of mitochondrial function. The data were presented with mean ± standard deviation. Student's *t*-test was used for statistical analysis. *$p < 0.05$.

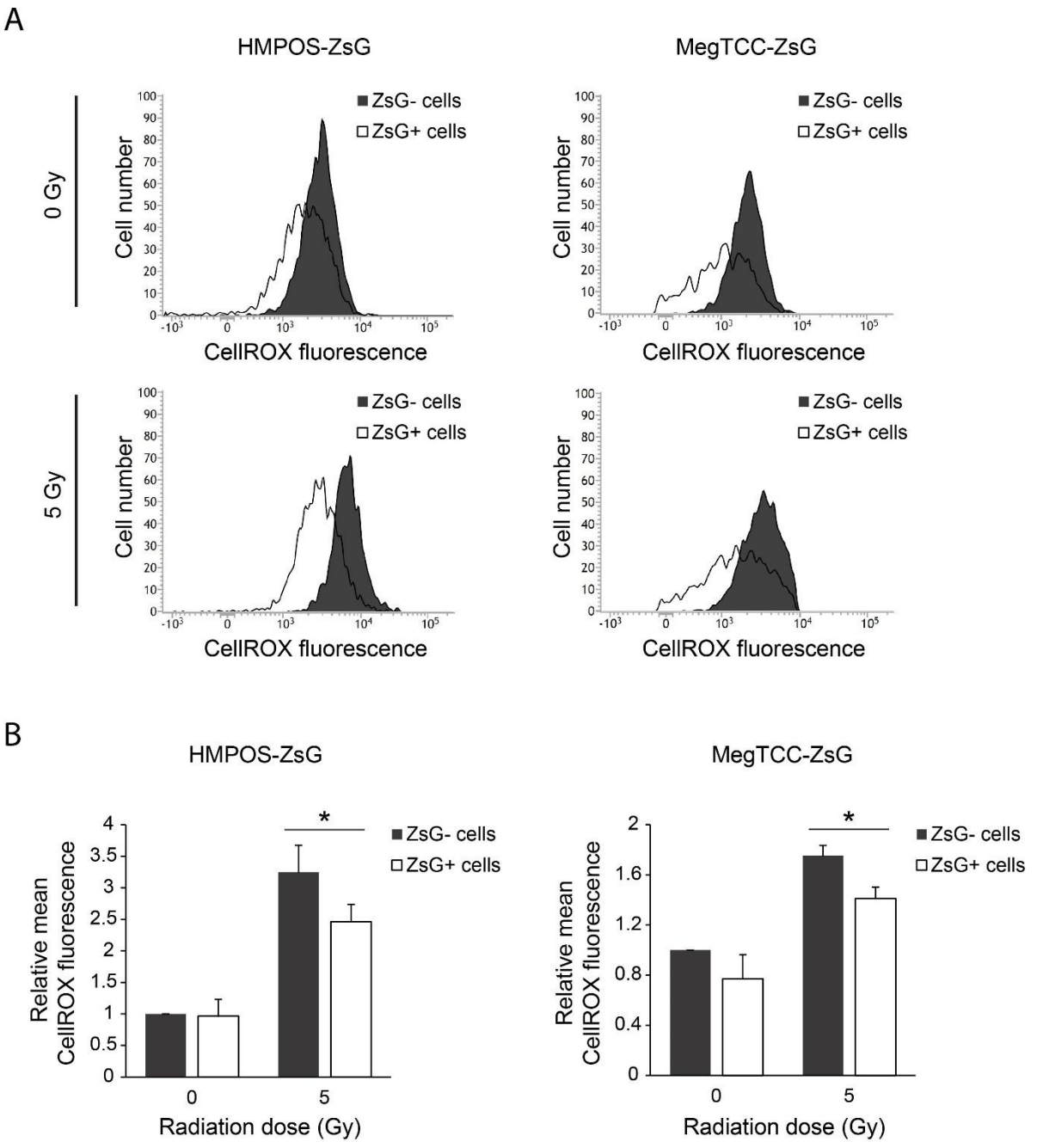

Figure II-7. ROS accumulation in ZsG$^+$ cells after X-irradiation

(A) Flow cytometric analysis of ROS accumulation in ZsG$^-$ and ZsG$^+$ cells after 0 or 5 Gy X-irradiation. (B) Comparative analysis using the results of ROS accumulation normalized to the CellROX fluorescence of ZsG$^-$ cells of HMPOS-ZsG without X-irradiation. The data were presented with mean ± standard deviation. Tukey's multiple comparison test was used for statistical analysis. *$p < 0.05$.

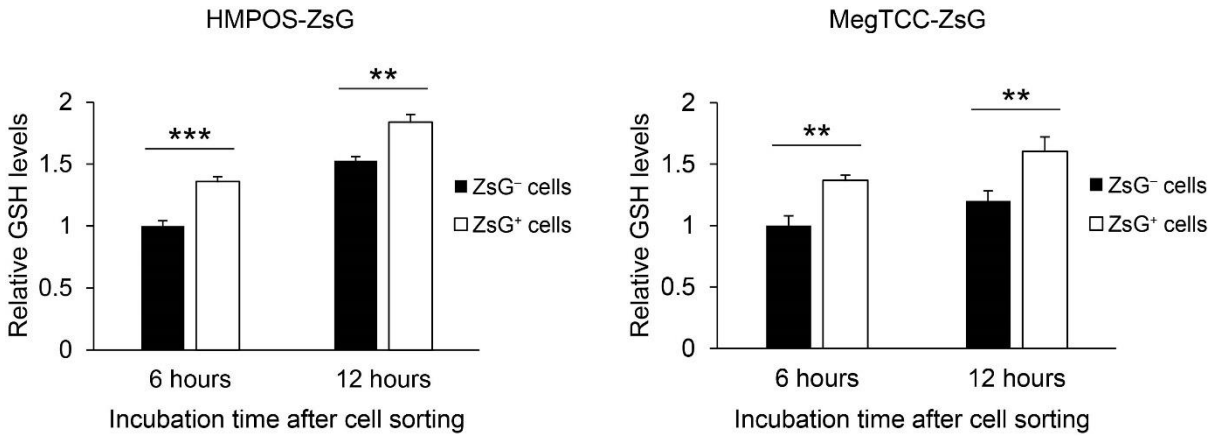

Figure II-8. GSH contents of ZsG$^+$ cells

Relative GSH contents of ZsG$^-$ and ZsG$^+$ cells after 6 or 12 hours of cell sorting were determined in HMPOS-ZsG and MegTCC-ZsG. The data were presented with mean ± standard deviation. Tukey's multiple comparison test was used for statistical analysis. $^{**}p < 0.01$ and $^{***}p < 0.001$.

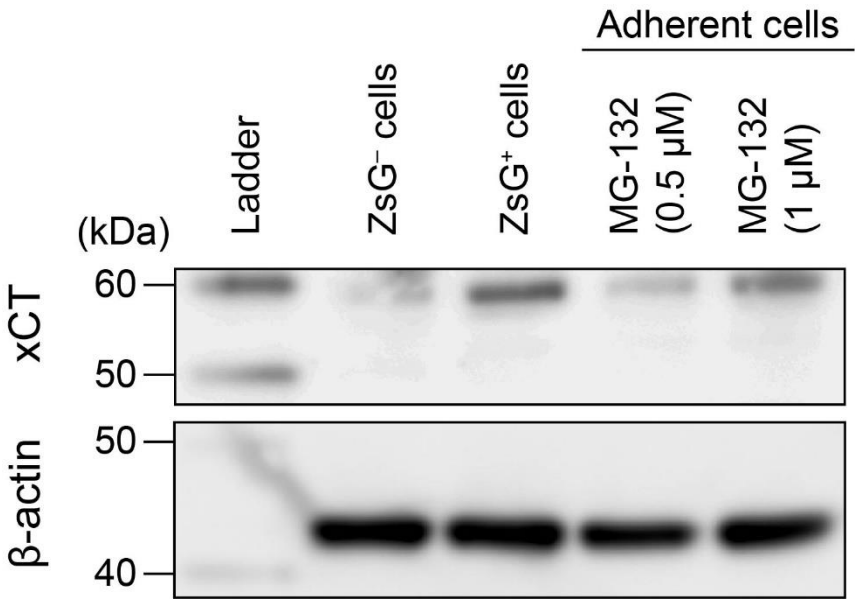

Figure II-9. Protein level of xCT at low proteasome activity in HMPOS-ZsG

Western blot analysis was performed to compare protein level of xCT (molecular weight, 58 kDa) between groups: ZsG^- cells, ZsG^+ cells, and adherent cells which were cultured with 0.5-μM MG-132 or 1-μM MG-132 in HMPOS-ZsG. β-actin (molecular weight, 44 kDA) was employed as a loading control of Western blot analysis.

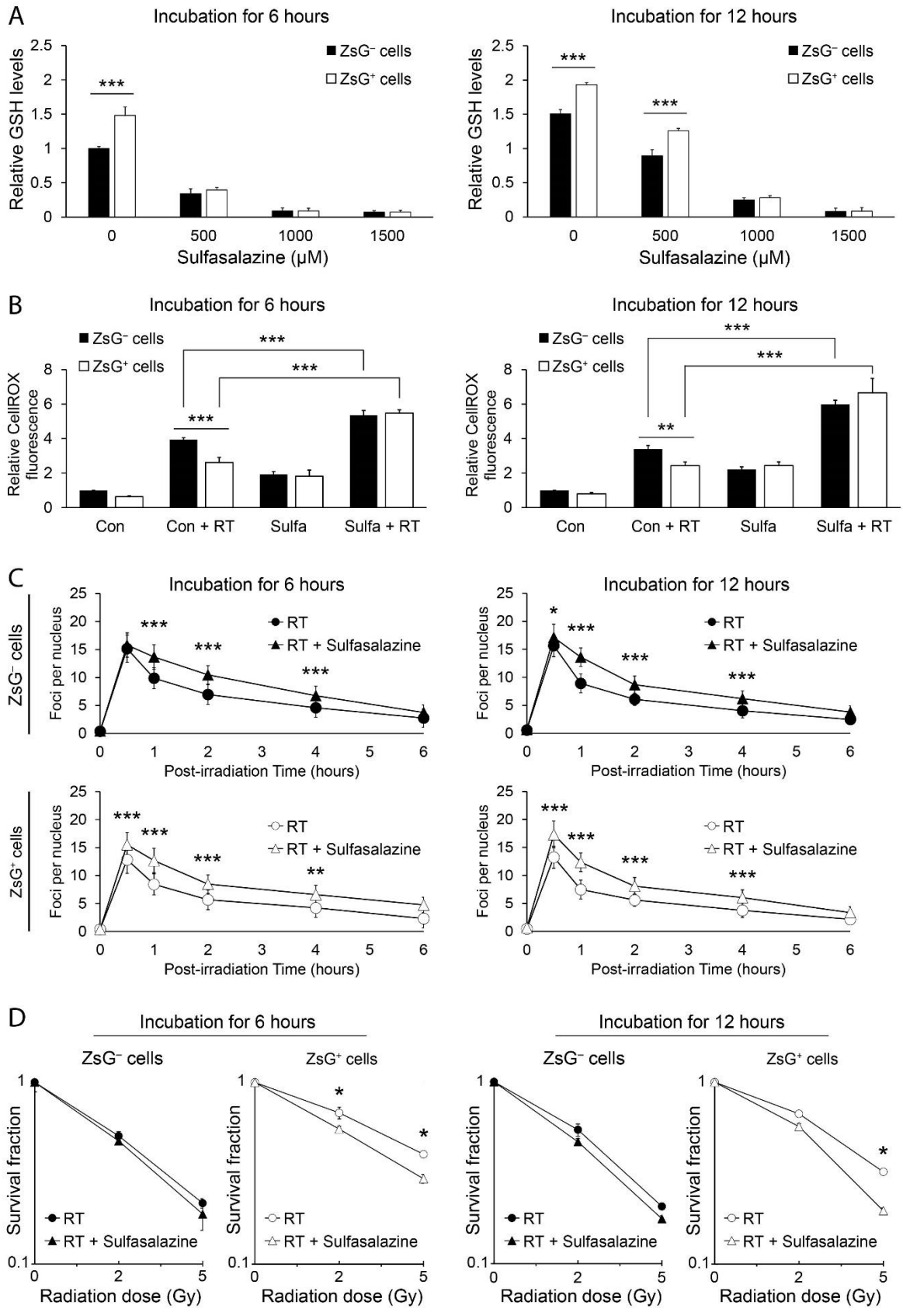
A
Incubation for 6 hours
Incubation for 12 hours
Relative GSH levels
ZsG⁻ cells
ZsG⁺ cells
Sulfasalazine (μM)
B
Incubation for 6 hours
Incubation for 12 hours
Relative CellROX fluorescence
Con
Con + RT
Sulfa
Sulfa + RT
C
Incubation for 6 hours
Incubation for 12 hours
ZsG⁻ cells
ZsG⁺ cells
Foci per nucleus
RT
RT + Sulfasalazine
Post-irradiation Time (hours)
D
Incubation for 6 hours
Incubation for 12 hours
ZsG⁻ cells
ZsG⁺ cells
Survival fraction
RT
RT + Sulfasalazine
Radiation dose (Gy)

Figure II-10. Role of xCT in the radio-resistance of ZsG^+ cells in HMPOS-ZsG

(A) GSH contents of ZsG^- and ZsG^+ cells after treatment with different concentration of sulfasalazine. (B) Accumulation of intracellular ROS after X-irradiation and treatment with 1,000-μM sulfasalazine (Sulfa) in ZsG^- and ZsG^+ cells. (C) Change of DSB which is caused by X-irradiation after incubation with 1,000-μM sulfasalazine in ZsG^- and ZsG^+ cells. (D) Radiation survival curves showing radiosensitizing effects of 1,000-μM sulfasalazine. The data were presented with mean ± standard deviation. Tukey's multiple comparison test was used for statistical analysis. $*p < 0.05$, $**p < 0.01$, and $***p < 0.001$.

DISCUSSION

This study investigated the mechanism of radio-resistance in the HMPOS and MegTCC cells with low proteasome activity. According to the previous research, tumor cells with low proteasome activity are radio-resistant in human tumor cells, but this is still unclear in canine tumor cells. Furthermore, the mechanism of the radio-resistance in these cells is not revealed in both human and canine tumor cells. Herein, our findings, for the first time, unveil the mechanism of radio-resistance in canine tumor cells with low proteasome activity.

After X-irradiation, the ratio of the survived ZsG^+ cells dose-dependently increased in adherent cell culture showing the possibility that ZsG^+ cells are radio-resistant. In addition, the actual radio-resistance was evaluated using clonogenic survival assay in ZsG^- and ZsG^+ cells, and ZsG^+ cells showed higher radio-resistance than ZsG^- cells did. In the first chapter, ZsG^+ cells were isolated based on the property of low proteasome activity and showed CSC-like properties. The increased ratio of the survived ZsG^+ cells and their radio-resistance are corresponding to previous reports of human tumor cells such as osteosarcoma, squamous cell carcinomas, prostate cancer, and colorectal cancer where tumor cells with low proteasome activity exhibited CSC-like properties and radio-resistance [Tamari *et al*., 2014; Lagadec *et al*., 2014b; Munakata *et al*., 2016; Della Donna *et al*., 2012; Kano *et al*., 2014].

In the present study, ZsG^+ cells exhibited lower number of 53BP1 foci per nucleus than ZsG^- cells after 0.5 or 1 hour of irradiation. The accumulation of 53BP1 in nucleus is related to DSB because this occurs following an activation of RNF8–RNF168-mediated ubiquitylation cascade which is a downstream of γH2AX; an indicator of DSB [Panier and Boulton, 2014]. Furthermore, foci formation of 53BP1 is similar to the that of γH2AX after exposure to X-irradiation in human stem cells [Tsvetkova *et al*., 2017]. Therefore, the results in this study indicate low level of initial DNA damage in ZsG^+ cells and correspond to

previous studies where CSCs have showed low foci formation of 53BP1 after treated by radiation [Deguchi *et al*., 2019; Shimamura *et al*., 2018]. Low level of initial DNA damage was observed from radio-resistant human squamous cell carcinoma cells [Hanot *et al*., 2012] and radiosensitivity was correlated with initial DNA damage rather than residual DNA damage in eleven cell lines [Roos *et al*., 2000]. This is owing to high GSH contents and low ROS accumulation [Hanot *et al*., 2012; Kim *et al*., 2019]. In addition to the low ROS accumulation of ZsG^+ cells after irradiation, early responsive DNA repair like non-homologous end-joining (NHEJ) might be related to the low number of 53BP1 foci formation of ZsG^+ cells. The majority of initial DSB caused by radiation is repaired by NHEJ process [Ahmed *et al*., 2018], and NHEJ has short half-life of 5–30 minutes [Morgan and Lawrence, 2015]. The NHEJ may already have started the repair process of DSB before 30 minutes of irradiation. The gradient slope of 53BP1 after 30 minutes of irradiation seems lower in the ZsG^- cells than that in the ZsG^+ cells. Nevertheless, confirmation of the 53BP1 foci formation before 30 minutes of X-irradiation is required to evaluate the contribution of DNA repairs to the results of this study.

DNA contents of the cells were analyzed using propidium iodide staining, and diploid DNA peaks were observed in ZsG^- and ZsG^+ cells. The cells did not show non-diploid DNA peak. According to previous studies, tumor cells which have non-diploid DNA tend to exhibit radio-resistance and poor outcome of radiation therapy in human tumors [Gauwitz *et al*., 1994; Raybaud *et al*., 2000]. This is because that increase of DNA ploidy offer tumors chances of rapid evolution to therapy resistant phenotype [Coward and Harding, 2014]. However, our study did not detect non-diploidy of ZsG^- or ZsG^+ cells indicating that the radio-resistance of ZsG^+ cells is not related to the DNA ploidy.

Mitochondrial function of the ZsG^- and ZsG+ cells was analyzed in this study. Results of the Mito stress test exhibited that mitochondrial function of ZsG^+ cells is not up-regulated

compared with that of ZsG^- cells in this study. The results of the mitochondrial function are in accordance with some previous studies [Sun *et al*., 2017; Palorini *et al*., 2014] that CSCs showed low mitochondrial metabolism, and these cells featured up-regulated glycolytic metabolism. Also, recent studies have reported that oxidative phosphorylation and glycolysis of CSCs are interchangeable, and CSCs choose which side to use for energy production depending on tumor microenvironment [Zhu *et al*., 2020; Walsh *et al*., 2019]. Therefore, ZsG^+ cells could more exploit glycolysis to produce energy compared with oxidative phosphorylation and may change the way for energy generation according to tumor microenvironment.

In the present study, ZsG^+ cells exhibited lower accumulation of cellular ROS than ZsG^- cells after exposure to X-irradiation in both HMPOS-ZsG and MegTCC-ZsG. Mildly up-regulated ROS in tumor cells contribute to tumor proliferation, survival, and oncogene expression as well as antitumor gene suppression by modulating signaling pathways [Perillo *et al*., 2020]. However, excessive ROS accumulation results in DSB and cell death with oxidative cellular damage which can be caused by radiation [Reczek and Chandel, 2017; Kim *et al*., 2019]. Therefore, keeping low ROS level after irradiation is related to survival and radio-resistance of tumor cells like ZsG^+ cells [Tuy *et al*., 2021]. To avoid the excessive ROS accumulation after irradiation, CSCs maintain low ROS levels regulating production and scavenging of ROS through altered expression of GSH contents and antioxidant proteins, and activation of ROS-dependent signaling pathways [Ding *et al*., 2015].

Total GSH contents were measured in cells, and ZsG^+ cells showed larger amount of GSH contents than ZsG^- cells did. According to a previous report, GSH depletion generates accumulation of reactive species such as ROS and activates apoptotic signaling pathways, resulting in apoptotic cell death [Franco and Cidlowski, 2009]. Thus, increase of ROS production after irradiation would depletes intracellular GSH contents and induces apoptotic

cell death [Yamamori *et al*., 2012]. In human breast cancer cells, GSH reduction induced radio-sensitization with increased intracellular ROS levels [Cobler *et al*., 2018]. Moreover, up-regulated GSH level is important to maintain cancer stemness in CSCs, and inhibition of GSH synthesis decreased cancer stem-like properties and viability of CSCs in human pancreatic cancer cells [Jagust *et al*., 2020]. Accordingly, GSH is a promising target of CSCs in radiation therapy.

In the Western blot analysis, the protein level of xCT was high in the ZsG^+ cells and adherent cells which were treated with the proteasome inhibitor indicating a relationship between protein level of xCT and proteasome activity. According to recent reports, xCT is degraded by proteasome activity after ubiquitination, and the degradation is stabilized by forming a trimetric complex with CD44 variant, OTUB1 which is a family of deubiquitinase, thereby contributing to protein stability of xCT [Liu *et al*., 2019; Gan, 2019]. This indicates that the xCT in ZsG^+ cells would be stabilized by low proteasome activity condition contributing to the reduced degradation of xCT. In future studies, the expression level of xCT and related transcriptional factors in ZsG^+ cells should be investigated regarding different proteasome activities for a better understanding of the mechanisms.

Subsequently, the role of xCT was evaluated in the GSH synthesis and the radio-resistance of ZsG^+ cells in HMPOS-ZsG. Sulfasalazine as a xCT inhibitor decreased the level of GSH contents and eliminated the difference of the accumulation of intracellular ROS after X-irradiation between $ZsG^–$ and ZsG^+ cells. In addition, sulfasalazine enhanced DSB of ZsG^+ cells after X-irradiation, especially initial DSB of ZsG^+ cells compared with that of $ZsG^–$ cells. Finally, sulfasalazine induced radiosensitization of ZsG^+ cells effectively. According to recent studies, inhibition of xCT using sulfasalazine is related to the sensitivity of canine tumor cells to oxidative damages such as H_2O_2 [Tanabe *et al*., 2021], and xCT is up-regulated in spheroid cells in a canine hepatocellular carcinoma cell line [Itoh *et al*., 2021]. Also,

sulfasalazine exhibits antitumor effects to CSCs expressing CSC marker such as CD133. CSCs which are CD133-positive maintain reduced oxidative stress by stabilizing xCT [Jang *et al*., 2017; Song *et al*., 2017]. This results in sensitization of the CSCs to antitumor drugs, decreased the CSC population, and prolonged survival [Song *et al*., 2017; Thanee *et al*., 2021; Haryu *et al*., 2018]. Our study showed that ZsG^+ cells highly express *CD133* in the first chapter and ZsG^+ have high level of xCT protein at low proteasome activity condition. These results explain together why sulfasalazine showed effects of targeting ZsG^+ cells. In addition to the previous studies, the present study further elucidated that the up-regulated xCT and GSH contents contribute to the radio-resistance of canine CSCs with low proteasome activity, making the cells tolerate to oxidative damage and DSB caused by X-irradiation. Thereby, this study demonstrate that the xCT is a promising target for the radio-resistance of canine tumor cells with low proteasome activity.

In conclusion, this study revealed that the radio-resistance and its mechanism of canine tumor cells with low proteasome activity in which GSH contents are up-regulated affecting low ROS accumulation and low DBS after X-irradiation. Sulfasalazine by reducing GSH contents successfully radiosensitized canine osteosarcoma cells with low proteasome activity which have high protein level of xCT. Therefore, xCT would be an effective target for the radio-resistance of CSCs in canine osteosarcoma cells.

SUMMARY

Radio-resistance of CSCs has been associated with treatment failure of radiation therapy in canine tumor cells. In the first chapter, isolation of canine CSCs was succeeded using a property of low proteasome activity, ZsG^+ cells. However, radio-resistance and its mechanism are still not clear in tumor cells with low proteasome activity to target CSCs in radiation therapy. The aim of this study was to evaluate the radio-resistance of ZsG^+ cells and elucidate its radio-resistance mechanism searching for a potential target of CSCs using HMPOS-ZsG and MegTCC-ZsG. The ZsG^+ cells were isolated using flow cytometric cell sorter and compared with ZsG^- cells. Radio-resistance of the ZsG^+ cells was evaluated using a flow cytometer, fluorescence microscopy, and clonogenic survival assay. Mechanism of the radio-resistance was evaluated by immunocytochemistry of 53BP1, DNA ploidy analysis, Cell mito stress test, reactive oxygen production detection, GSH assay, and Western blot analysis. Sulfasalazine was employed as an inhibitor of xCT which is related to GSH synthesis. Radio-resistance of the ZsG^+ cells were significantly higher than that of the ZsG^- cells. As mechanisms of the radio-resistance, ZsG^+ cells showed that low 53BP1 foci formation after X-irradiation, low mitochondrial respiration, low accumulation of ROS after X-irradiation, and low GSH contents, without any abnormality in DNA ploidy. ZsG^+ cells in HMPOS-ZsG showed high protein level of xCT which is a cystine/glutamate antiporter related to GSH synthesis, and the ZsG^+ cells were successfully radiosensitized by sulfasalazine. This is because sulfasalazine depleted GSH contents, thereby increasing ROS accumulation and 53BP1 foci formation after X-irradiation in ZsG^+ cells. In conclusion, canine tumor cells with low proteasome activity have high radio-resistance with increased GSH contents. Also,

sulfasalazine is a valuable radiosensitizer and xCT would be a promising target for CSCs in canine osteosarcoma cells.

GENERAL CONCLUSION

The objective of this study was to visualize CSCs using a property of low proteasome activity for identification and isolation of CSCs, and to reveal the radio-resistance mechanism of CSCs using the visualization system searching for an effective target of CSCs. In the present study, canine tumor cells with low proteasome activity was visualized, which were named "ZsG^+ cells", and the property of low proteasome activity in canine CSCs was confirmed using spheroid cells which are CSC rich. Then, CSC-like properties were investigated using the isolated ZsG^+ cells. Subsequently, radiosensitivity of the ZsG^+ cells was evaluated to confirm whether they have same radiosensitivity with human CSCs, and mechanism of the radio-sensitivity of ZsG^+ cells was explored. Finally, following the results about the radiosensitivity mechanism, an appropriate drug was chosen and its radiosensitizing effects were evaluated in ZsG^+ cells.

In the first chapter, canine tumor cells were genetically engineered to express green fluorescent protein ZsGreen1 connected to proteasome degron cODC using the lentiviral system. The mode of the visualization system was confirmed using MG-132 which is a proteasome inhibitor and increased the green fluorescence intensity of the canine tumor cells. The visualized canine tumor cells with low proteasome activity or ZsG^+ cells could be identified by their green fluorescence and isolated using flow cytometric cell sorter. Also, spheroid cells which are CSC rich showed lower proteasome activity than adherent cells which have only few CSCs, showing an applicability of the visualization system to canine CSCs. The ZsG^+ cells showed symmetric cell division with or without phenotype change and asymmetric cell division like CSCs. This data demonstrated how the population of CSCs decreases after isolation visually. In addition, ZsG^+ cells exhibited low G0/G1 phase of cell

cycle indicating their cell dividing characteristics. The result of RNA sequencing suggested up-regulation of several CSC markers in ZsG^+ cells and they were correlated to the results of qPCR. Among the CSC markers, ZsG^+ highly expressed *CD133* in both HMPOS-ZsG and MegTCC-ZsG. In HMPOS-ZsG, the function of ABCG2 was up-regulated in ZsG^+ cells. Furthermore, ZsG^+ cells showed higher tumorigenic capacity than ZsG^- cells, and in the histological analysis, distribution of ZsG^+ cells was observed in tumor tissues derived from ZsG^+ cells rather than from ZsG^- cells. The ratio of the ZsG+ cells in tumor tissues was highest in metastasis region which was followed by core region, periphery region, and necrotic region. These results exhibited that canine CSCs were successfully visualized and isolated using their property of low proteasome activity.

In the second chapter, by using the CSC visualization, the radio-resistance of ZsG^+ cells and the radio-resistance mechanism were evaluated to establish effective strategy for targeting CSCs in radiation therapy. ZsG^+ cells were identified and isolated using flow cytometric cell sorter based on their level of ZsGreen1 fluorescence intensity. Then, radio-resistance of ZsG^+ cells was investigated by confocal microscopy, flow cytometry, and clonogenic survival assay. The radio-resistance mechanism was examined using 53BP1 immunostaining, DNA ploidy analysis, Cell mito stress test, reactive oxygen production detection, GSH assay, and Western blot analysis. Sulfasalazine which is an inhibitor of xCT and prevents GSH synthesis was employed as a radiosensitizer. The results showed that ZsG^+ cells are more radio-resistance than ZsG^- cells with low initial DNA damage after X-irradiation, low intracellular ROS accumulation after X-irradiation, and high GSH contents. The sulfasalazine successfully radiosensitized ZsG^+ cells. The effects of sulfasalazine decreased GSH contents and increased intracellular ROS accumulation after exposure to radiation in ZsG^+ cells. In addition, the sulfasalazine increased DNA damage from X-irradiation in ZsG^+ cells. These results suggest that canine tumor cells with low proteasome

activity are radio-resistant with high expression level of GSH. Moreover, the sulfasalazine is an effective radiosensitizer for canine CSCs in radiation therapy, and xCT could be utilized as a valuable target of CSCs in canine osteosarcoma cells.

To summarize this dissertation, imaged canine tumor cells based on their low proteasome activity were successfully isolated and were demonstrated to have CSC-like properties. Furthermore, by utilizing the CSC visualization, the radio-resistance and its mechanism, up-regulation of GSH, of canine CSCs were revealed. Finally, the present study discovered that xCT would be an effective target, and sulfasalazine can be a radiosensitizer of CSCs in canine osteosarcoma cells.

REFERENCES

Adams, J. 2003. The proteasome: Structure, function, and role in the cell. *Cancer Treat. Rev.* **29**: 3–9.

Adikrisna, R., Tanaka, S., Muramatsu, S., Aihara, A., Ban, D., Ochiai, T., Irie, T., Kudo, A., Nakamura, N., Yamaoka, S. and Arii, S. 2012. Identification of Pancreatic Cancer Stem Cells and Selective Toxicity of Chemotherapeutic Agents. *Gastroenterology*. **143**: 234-245.e7.

Aguilar-Gallardo, C. and Simón, C. 2013. Cells, stem cells, and cancer stem cells. *Semin. Reprod. Med.* **31**: 5–13.

Ahmed, E. A., Rosemann, M. and Scherthan, H. 2018. NHEJ Contributes to the Fast Repair of Radiation-induced DNA Double-strand Breaks at Late Prophase I Telomeres. *Health Phys.* **115**: 102–107.

Al-Hajj, M., Wicha, M. S., Benito-Hernandez, A., Morrison, S. J. and Clarke, M. F. 2003. Prospective identification of tumorigenic breast cancer cells. *Proc. Natl. Acad. Sci.* **100**: 3983–3988.

Arnold, C. R., Mangesius, J., Skvortsova, I.-I. and Ganswindt, U. 2020. The Role of Cancer Stem Cells in Radiation Resistance. *Front. Oncol.* **10**: 1–12.

Ayob, A. Z. and Ramasamy, T. S. 2018. Cancer stem cells as key drivers of tumour

progression. *J. Biomed. Sci.* **25**: 20.

Barroga, E. F., Kadosawa, T., Okumura, M. and Fujinaga, T. 1999. Establishment and Characterization of the Growth and Pulmonary Metastasis of a Highly Lung Metastasizing Cell Line from Canine Osteosarcoma in Nude Mice. *J. Vet. Med. Sci.* **61**: 361–367.

Basu-Roy, U., Basilico, C. and Mansukhani, A. 2013. Perspectives on cancer stem cells in osteosarcoma. *Cancer Lett.* **338**: 158–167.

Batlle, E. and Clevers, H. 2017. Cancer stem cells revisited. *Nat. Med.* **23**: 1124–1134.

Begicevic, R.-R. and Falasca, M. 2017. ABC Transporters in Cancer Stem Cells: Beyond Chemoresistance. *Int. J. Mol. Sci.* **18**: 2362.

Bonnet, D. and Dick, J. E. 1997. Human acute myeloid leukemia is organized as a hierarchy that originates from a primitive hematopoietic cell. *Nat. Med.* **3**: 730–737.

Brush, J. M., Kim, K., Sayre, J. W., McBride, W. H. and Iwamoto, K. S. 2009. Imaging of radiation effects on cellular 26S proteasome function in situ. *Int. J. Radiat. Biol.* **85**: 483–94.

Bu, P., Chen, K., Lipkin, S. M. and Shen, X. 2013. Asymmetric division: a marker for cancer stem cells? *Oncotarget*. **4**: 950–951.

Cao, L., Zhou, Y., Zhai, B., Liao, J., Xu, W., Zhang, R., Li, J., Zhang, Y., Chen, L., Qian, H., Wu, M. and Yin, Z. 2011. Sphere-forming cell subpopulations with cancer stem cell

properties in human hepatoma cell lines. *BMC Gastroenterol.* **11**: 71.

Chang, J. C. 2016. Cancer stem cells. *Medicine (Baltimore).* **95**: S20–S25.

Chen, D., Jiao, Y. and Torquato, S. 2014. A Cellular Automaton Model for Tumor Dormancy: Emergence of a Proliferative Switch. *PLoS One*. **9**: e109934.

Chen, Z. Y., Wang, X., Zhou, Y., Offner, G. and Tseng, C. C. 2005. Destabilization of Krüppel-like factor 4 protein in response to serum stimulation involves the ubiquitin-proteasome pathway. *Cancer Res.* **65**: 10394–10400.

Chio, I. I. C. and Tuveson, D. A. 2017. ROS in Cancer: The Burning Question. *Trends Mol. Med.* **23**: 411–429.

Cho, Y. and Kim, Y. K. 2020. Cancer Stem Cells as a Potential Target to Overcome Multidrug Resistance. *Front. Oncol.* **10**: 1–10.

Cobler, L., Zhang, H., Suri, P., Park, C. and Timmerman, L. A. 2018. xCT inhibition sensitizes tumors to γ-radiation via glutathione reduction. *Oncotarget*. **9**: 32280–32297.

Collins, A. T., Berry, P. A., Hyde, C., Stower, M. J. and Maitland, N. J. 2005. Prospective Identification of Tumorigenic Prostate Cancer Stem Cells. *Cancer Res.* **65**: 10946–10951.

Collins, G. A. and Goldberg, A. L. 2017. The Logic of the 26S Proteasome. *Cell*. **169**: 792–806.

Combs, J. A. and Denicola, G. M. 2019. The non-essential amino acid cysteine becomes essential for tumor proliferation and survival. *Cancers (Basel).* **11**: 678.

Cooper, J. K., Sykes, G., King, S., Cottrill, K., Ivanova, N. V., Hanner, R. and Ikonomi, P. 2007. Species identification in cell culture: a two-pronged molecular approach. *Vitr. Cell. Dev. Biol. - Anim.* **43**: 344–351.

Costa, C. D., Justo, A. A., Kobayashi, P. E., Story, M. M., Palmieri, C., Laufer Amorim, R. and Fonseca-Alves, C. E. 2019. Characterization of OCT3/4, Nestin, NANOG, CD44 and CD24 as stem cell markers in canine prostate cancer. *Int. J. Biochem. Cell Biol.* **108**: 21–28.

Coward, J. and Harding, A. 2014. Size Does Matter: Why Polyploid Tumor Cells are Critical Drug Targets in the War on Cancer. *Front. Oncol.* **4**: 1–15.

Crawford, L. J., Walker, B. and Irvine, A. E. 2011. Proteasome inhibitors in cancer therapy. *J. Cell Commun. Signal.* **5**: 101–110.

Deguchi, T., Hosoya, K., Murase, Y., Koangyong, S., Kim, S. and Okumura, M. 2019. Analysis of radiosensitivity of cancer stem-like cells derived from canine cancer cell lines. *Vet. Comp. Oncol.* **17**: 119–129.

Delaney, G., Jacob, S., Featherstone, C. and Barton, M. 2005. The role of radiotherapy in cancer treatment: Estimating optimal utilization from a review of evidence-based clinical guidelines. *Cancer*. **104**: 1129–1137.

Della Donna, L., Lagadec, C. and Pajonk, F. 2012. Radioresistance of prostate cancer cells with low proteasome activity. *Prostate*. **72**: 868–874.

Deng, L., Meng, T., Chen, L., Wei, W. and Wang, P. 2020. The role of ubiquitination in tumorigenesis and targeted drug discovery. *Signal Transduct. Target. Ther.* **5**: 11.

Desouky, O., Ding, N. and Zhou, G. 2015. Targeted and non-targeted effects of ionizing radiation. *J. Radiat. Res. Appl. Sci.* **8**: 247–254.

Diehn, M., Cho, R. W., Lobo, N. A., Kalisky, T., Dorie, M. J., Kulp, A. N., Qian, D., Lam, J. S., Ailles, L. E., Wong, M., Joshua, B., Kaplan, M. J., Wapnir, I., Dirbas, F. M., Somlo, G., Garberoglio, C., Paz, B., Shen, J., Lau, S. K., Quake, S. R., Brown, J. M., Weissman, I. L. and Clarke, M. F. 2009. Association of reactive oxygen species levels and radioresistance in cancer stem cells. *Nature*. **458**: 780–783.

Ding, S., Li, C., Cheng, N., Cui, X., Xu, X. and Zhou, G. 2015. Redox regulation in cancer stem cells. *Oxid. Med. Cell. Longev.* **2015**: 1–11.

Dixon, S. J., Lemberg, K. M., Lamprecht, M. R., Skouta, R., Zaitsev, E. M., Gleason, C. E., Patel, D. N., Bauer, A. J., Cantley, A. M., Yang, W. S., Morrison, B. and Stockwell, B. R. 2012. Ferroptosis: an iron-dependent form of nonapoptotic cell death. *Cell*. **149**: 1060–72.

Enjoji, S., Yabe, R., Fujiwara, N., Tsuji, S., Vitek, M. P., Mizuno, T., Nakagawa, T., Usui, T., Ohama, T. and Sato, K. 2015. The therapeutic effects of SET/I2PP2A inhibitors on canine

melanoma. *J. Vet. Med. Sci.* **77**: 1451–1456.

Feng, H.-L., Liu, Y.-Q., Yang, L.-J., Bian, X.-C., Yang, Z.-L., Gu, B., Zhang, H., Wang, C.-J., Su, X.-L. and Zhao, X.-M. 2010. Expression of CD133 correlates with differentiation of human colon cancer cells. *Cancer Biol. Ther.* **9**: 216–223.

Ferletta, M., Grawé, J. and Hellmén, E. 2011. Canine mammary tumors contain cancer stem-like cells and form spheroids with an embryonic stem cell signature. *Int. J. Dev. Biol.* **55**: 791–799.

Franco, R. and Cidlowski, J. A. 2009. Apoptosis and glutathione: Beyond an antioxidant. *Cell Death Differ.* **16**: 1303–1314.

Frisch, S. M. and Francis, H. 1994. Disruption of epithelial cell-matrix interactions induces apoptosis. *J. Cell Biol.* **124**: 619–626.

Furuyama, T., Tanaka, S., Shimada, S., Akiyama, Y., Matsumura, S., Mitsunori, Y., Aihara, A., Ban, D., Ochiai, T., Kudo, A., Fukamachi, H., Arii, S., Kawaguchi, Y. and Tanabe, M. 2016. Proteasome activity is required for the initiation of precancerous pancreatic lesions. *Sci. Rep.* **6**: 27044.

Gan, B. 2019. DUBbing Ferroptosis in Cancer Cells. *Cancer Res.* **79**: 1749–1750.

Gauwitz, M. D., Pollack, A., El-naggar, A. K., Terry, N. H. A., Eschenbach, A. C. and Zagars, G. K. 1994. The prognostic significance of DNA ploidy in clinically localized prostate cancer

treated with radiation therapy. *Int. J. Radiation Oncology Biol. Phys.* **28**: 821–828.

German, A. J., Halladay, L. J. and Noble, P. J. M. 2010. First-choice therapy for dogs presenting with diarrhoea in clinical practice. *Vet. Rec.* **167**: 810–814.

Gil, M., Seshadri, M., Komorowski, M. P., Abrams, S. I. and Kozbor, D. 2013. Targeting CXCL12/CXCR4 signaling with oncolytic virotherapy disrupts tumor vasculature and inhibits breast cancer metastases. *Proc. Natl. Acad. Sci.* **110**: E1291–E1300.

Goodell, M. A., Brose, K., Paradis, G., Conner, A. S. and Mulligan, R. C. 1996. Isolation and functional properties of murine hematopoietic stem cells that are replicating in vivo. *J. Exp. Med.* **183**: 1797–1806.

Gout, P. W., Buckley, A. R., Simms, C. R. and Bruchovsky, N. 2001. Sulfasalazine, a potent suppressor of lymphoma growth by inhibition of the x_C^- cystine transporter: a new action for an old drug. *Leukemia*. **15**: 1633–1640.

Hanot, M., Boivin, A., Malésys, C., Beuve, M., Colliaux, A., Foray, N., Douki, T., Ardail, D. and Rodriguez-Lafrasse, C. 2012. Glutathione depletion and carbon ion radiation potentiate clustered DNA lesions, cell death and prevent chromosomal changes in cancer cells progeny. *PLoS One*. **7**: e44367.

Haryu, S., Saito, R., Jia, W., Shoji, T., Mano, Y., Sato, A., Kanamori, M., Sonoda, Y., Sampetrean, O., Saya, H. and Tominaga, T. 2018. Convection-enhanced delivery of sulfasalazine prolongs survival in a glioma stem cell brain tumor model. *J. Neurooncol.* **136**:

23–31.

Hayashi, K., Tamari, K., Ishii, H., Konno, M., Nishida, N., Kawamoto, K., Koseki, J., Fukusumi, T., Kano, Y., Nishikawa, S., Miyo, M., Noguchi, K., Ogawa, H., Hamabe, A., Seo, Y., Doki, Y., Mori, M. and Ogawa, K. 2014. Visualization and characterization of cancer stem-like cells in cervical cancer. *Int. J. Oncol.* **45**: 2468–2474.

He, X., Marchionni, L., Hansel, D. E., Yu, W., Sood, A., Yang, J., Parmigiani, G., Matsui, W. and Berman, D. M. 2009. Differentiation of a Highly Tumorigenic Basal Cell Compartment in Urothelial Carcinoma. *Stem Cells*. **27**: 1487–1495.

Inoue, K., Ohashi, E., Kadosawa, T., Hong, S.-H., Matsunaga, S., Mochizuki, M., Nishimura, R. and Sasaki, N. 2004. Establishment and characterization of four canine melanoma cell lines. *J. Vet. Med. Sci.* **66**: 1437–1440.

Itoh, H., Tani, K., Sunahara, H., Nakaichi, M., Iseri, T., Horikirizono, H. and Itamoto, K. 2021. Sphere-forming cells display stem cell-like characteristics and increased xCT expression in a canine hepatocellular carcinoma cell line. *Res. Vet. Sci.* **139**: 25–31.

Jagust, P., Alcalá, S., Jr, B. S., Heeschen, C. and Sancho, P. 2020. Glutathione metabolism is essential for self-renewal and chemoresistance of pancreatic cancer stem cells. *World J. Stem Cells* **12**: 1410–1428.

Jang, H. H. 2018. Regulation of protein degradation by proteasomes in cancer. *J. Cancer Prev.* **23**: 153–161.

Jang, J. W., Song, Y., Kim, S. H., Kim, J. and Seo, H. R. 2017. Potential mechanisms of CD133 in cancer stem cells. *Life Sci.* **184**: 25–29.

Jung, Y.-S., Vermeer, P. D., Vermeer, D. W., Lee, S.-J., Goh, A. R., Ahn, H.-J. and Lee, J. H. 2015. CD200: Association with cancer stem cell features and response to chemoradiation in head and neck squamous cell carcinoma. *Head Neck*. **37**: 327–335.

Kamal, A. F., Pranatha, D. Y., Sugito, W., Rahman, F., Susanto, E., Mariya, S. and Chen, W. M. 2018. Isolation, Culture and Characterization of Cancer Stem Cells from Primary Osteosarcoma. *Open Stem Cell J.* **5**: 1–13.

Kano, Y., Konno, M., Kawamoto, K., Tamari, K., Hayashi, K., Fukusumi, T., Satoh, T., Tanaka, S., Ogawa, K., Mori, M., Doki, Y. and Ishii, H. 2014. Novel drug discovery system for cancer stem cells in human squamous cell carcinoma of the esophagus. *Oncol. Rep.* **31**: 1133–1138.

Karbanová, J., Missol-Kolka, E., Fonseca, A.-V., Lorra, C., Janich, P., Hollerová, H., Jászai, J., Ehrmann, J., Kolář, Z., Liebers, C., Arl, S., Šubrtová, D., Freund, D., Mokrý, J., Huttner, W. B. and Corbeil, D. 2008. The stem cell marker CD133 (Prominin-1) is expressed in various human glandular epithelia. *J. Histochem. Cytochem.* **56**: 977–993.

Kawamura, K., Qi, F. and Kobayashi, J. 2018. Potential relationship between the biological effects of low-dose irradiation and mitochondrial ROS production. *J. Radiat. Res.* **59**: ii91–ii97.

Kim, J., Jung, J., Lee, S. J., Lee, J. S. and Park, M. J. 2012. Cancer stem-like cells persist in established cell lines through autocrine activation of EGFR signaling. *Oncol. Lett.* **3**: 607–612.

Kim, W., Lee, S., Seo, D., Kim, D., Kim, K., Kim, E. G., Kang, J. H., Seong, K. M., Youn, H. S. and Youn, B. H. 2019. Cellular stress responses in radiotherapy. *Cells*. **8**: 1105.

Kishimoto, T. E., Yashima, S., Nakahira, R., Onozawa, E., Azakami, D., Ujike, M., Ochiai, K., Ishiwata, T., Takahashi, K. and Michishita, M. 2017. Identification of tumor-initiating cells derived from two canine rhabdomyosarcoma cell lines. *J. Vet. Med. Sci.* **79**: 1155–1162.

Koppula, P., Zhuang, L. and Gan, B. 2021. Cystine transporter SLC7A11/xCT in cancer: ferroptosis, nutrient dependency, and cancer therapy. *Protein Cell*. **12**: 599–620.

Lagadec, C., Vlashi, E., Frohnen, P., Alhiyari, Y., Chan, M. and Pajonk, F. 2014a. The RNA-binding protein Musashi-1 regulates proteasome subunit expression in breast cancer- and glioma-initiating cells. *Stem Cells*. **32**: 135–144.

Lagadec, C., Vlashi, E., Bhuta, S., Lai, C., Mischel, P., Werner, M., Henke, M. and Pajonk, F. 2014b. Tumor cells with low proteasome subunit expression predict overall survival in head and neck cancer patients. *BMC Cancer*. **14**: 152.

Lathia, J. D., Gallagher, J., Myers, J. T., Li, M., Vasanji, A., McLendon, R. E., Hjelmeland, A. B., Huang, A. Y. and Rich, J. N. 2011. Direct in vivo evidence for tumor propagation by

glioblastoma cancer stem cells. *PLoS One*. **6**: e24807.

Lathia, J., Liu, H. and Matei, D. 2020. The clinical impact of cancer stem cells. *Oncologist* **25**: 123–131.

Lee, J., Sung, C. O., Lee, E. J., Do, I.-G., Kim, H.-C., Yoon, S. H., Lee, W. Y., Chun, H. K., Kim, K.-M. and Park, Y. S. 2012. Metastasis of neuroendocrine tumors are characterized by increased cell proliferation and reduced expression of the ATM gene. *PLoS One*. **7**: e34456.

Lenos, K. J. and Vermeulen, L. 2016. Cancer stem cells don't waste their time cleaning—low proteasome activity, a marker for cancer stem cell function. *Ann. Transl. Med.* **4**: 519–519.

Li, F., Zhou, K., Gao, L., Zhang, B., Li, W., Yan, W., Song, X., Yu, H., Wang, S., Yu, N. and Jiang, Q. 2016. Radiation induces the generation of cancer stem cells: A novel mechanism for cancer radioresistance (Review). *Oncol. Lett.* **12**: 3059–3065.

Li, Y., Wang, Z., Ajani, J. A. and Song, S. 2021. Drug resistance and cancer stem cells. *Cell Commun. Signal.* **19**: 19.

Lim, J. K. M., Delaidelli, A., Minaker, S. W., Zhang, H. F., Colovic, M., Yang, H., Negri, G. L., von Karstedt, S., Lockwood, W. W., Schaffer, P., Leprivier, G. and Sorensen, P. H. 2019. Cystine/glutamate antiporter xCT (SLC7A11) facilitates oncogenic RAS transformation by preserving intracellular redox balance. *Proc. Natl. Acad. Sci. U. S. A.* **116**: 9433–9442.

Linkous, A. G., Yazlovitskaya, E. M. and Hallahan, D. E. 2010. Cytosolic phospholipase A2

and lysophospholipids in tumor angiogenesis. *JNCI J. Natl. Cancer Inst.* **102**: 1398–1412.

Liu, T., Jiang, L., Tavana, O. and Gu, W. 2019. The deubiquitylase OTUB1 mediates ferroptosis via stabilization of SLC7A11. *Cancer Res.* **79**: 1913–1924.

Lyakhovich, A. and Lleonart, M. E. 2016. Bypassing mechanisms of mitochondria-mediated cancer stem cells resistance to chemo- and radiotherapy. *Oxid. Med. Cell. Longev.* **2016**: 1–10.

Ma, B., Lei, X., Guan, Y., Mou, L. S., Yuan, Y. F., Yue, H., Lu, Y., Xu, G. T. and Qian, J. 2011. Maintenance of retinal cancer stem cell-like properties through long-term serum-free culture from human retinoblastoma. *Oncol. Rep.* **26**: 135–143.

Ma, X.-L., Sun, Y.-F., Wang, B.-L., Shen, M.-N., Zhou, Y., Chen, J.-W., Hu, B., Gong, Z.-J., Zhang, X., Cao, Y., Pan, B., Zhou, J., Fan, J., Guo, W. and Yang, X.-R. 2019. Sphere-forming culture enriches liver cancer stem cells and reveals Stearoyl-CoA desaturase 1 as a potential therapeutic target. *BMC Cancer*. **19**: 760.

Majumdar, S. and Liu, S.-T. 2020. Cell division symmetry control and cancer stem cells. *AIMS Mol. Sci.* **7**: 82–101.

Marková, E., Schultz, N. and Belyaev, I. Y. 2007. Kinetics and dose-response of residual 53BP1/γ-H2AX foci: Co-localization, relationship with DSB repair and clonogenic survival. *Int. J. Radiat. Biol.* **83**: 319–329.

McCann, E., O'Sullivan, J. and Marcone, S. 2021. Targeting cancer-cell mitochondria and

metabolism to improve radiotherapy response. *Transl. Oncol.* **14**: 100905.

Michishita, M., Akiyoshi, R., Yoshimura, H., Katsumoto, T., Ichikawa, H., Ohkusu-Tsukada, K., Nakagawa, T., Sasaki, N. and Takahashi, K. 2011. Characterization of spheres derived from canine mammary gland adenocarcinoma cell lines. *Res. Vet. Sci.* **91**: 254–260.

Morgan, M. A. and Lawrence, T. S. 2015. Molecular pathways: Overcoming radiation resistance by targeting DNA damage response pathways. *Clin. Cancer Res.* **21**: 2898–2904.

Morrison, S. J. and Kimble, J. 2006. Asymmetric and symmetric stem-cell divisions in development and cancer. *Nature*. **441**: 1068–1074.

Mroczkiewicz, M., Winkler, K., Nowis, D., Placha, G., Golab, J. and Ostaszewski, R. 2010. Studies of the synthesis of all stereoisomers of MG-132 proteasome inhibitors in the tumor targeting approach. *J. Med. Chem.* **53**: 1509–1518.

Munakata, K., Uemura, M., Tanaka, S., Kawai, K., Kitahara, T., Miyo, M., Kano, Y., Nishikawa, S., Fukusumi, T., Takahashi, Y., Hata, T., Nishimura, J., Takemasa, I., Mizushima, T., Ikenaga, M., Kato, T., Murata, K., Carethers, J. M., Yamamoto, H., Doki, Y. and Mori, M. 2016. Cancer stem-like properties in colorectal cancer cells with low proteasome activity. *Clin. Cancer Res.* **22**: 5277–5286.

Nagane, M., Kanai, E., Shibata, Y., Shimizu, T., Yoshioka, C., Maruo, T. and Yamashita, T. 2018. Sulfasalazine, an inhibitor of the cystine-glutamate antiporter, reduces DNA damage repair and enhances radiosensitivity in murine B16F10 melanoma. *PLoS One*. **13**: e0195151.

Nemoto, Y., Maruo, T., Sato, T., Deguchi, T., Ito, T., Sugiyama, H., Ishikawa, T., Madarame, H., Watanabe, T., Shida, T. and Sahara, H. 2011. Identification of cancer stem cells derived from a canine lung adenocarcinoma cell line. *Vet. Pathol.* **48**: 1029–1034.

Ning, X., Du, Y., Ben, Q., Huang, L., He, X., Gong, Y., Gao, J., Wu, H., Man, X., Jin, J., Xu, M. and Li, Z. 2016. Bulk pancreatic cancer cells can convert into cancer stem cells (CSCs) in vitro and 2 compounds can target these CSCs. *Cell Cycle*. **15**: 403–412.

O'Brien, C. A., Pollett, A., Gallinger, S. and Dick, J. E. 2007. A human colon cancer cell capable of initiating tumour growth in immunodeficient mice. *Nature*. **445**: 106–110.

Olivares-Urbano, M. A., Griñán-Lisón, C., Marchal, J. A. and Núñez, M. I. 2020. CSC radioresistance: A therapeutic challenge to improve radiotherapy effectiveness in cancer. *Cells*. **9**: 1651.

Palorini, R., Votta, G., Balestrieri, C., Monestiroli, A., Olivieri, S., Vento, R. and Chiaradonna, F. 2014. Energy metabolism characterization of a novel cancer stem cell-like line 3AB-OS. *J. Cell. Biochem.* **115**: 368–379.

Pan, J., Zhang, Q., Wang, Y. and You, M. 2010. 26S Proteasome activity is down-regulated in lung cancer stem-like cells propagated in vitro. *PLoS One*. **5**: e13298.

Pang, L. Y., Gatenby, E. L., Kamida, A., Whitelaw, B. A., Hupp, T. R. and Argyle, D. J. 2014. Global gene expression analysis of canine osteosarcoma stem cells reveals a novel role for

COX-2 in tumour initiation. *PLoS One*. **9**: e83144.

Panier, S. and Boulton, S. J. 2014. Double-strand break repair: 53BP1 comes into focus. *Nat. Rev. Mol. Cell Biol.* **15**: 7–18.

Patrawala, L., Calhoun, T., Schneider-Broussard, R., Zhou, J., Claypool, K. and Tang, D. G. 2005. Side population is enriched in tumorigenic, stem-like cancer cells, whereas ABCG2 + and ABCG2 − cancer cells are similarly tumorigenic. *Cancer Res.* **65**: 6207–6219.

Perillo, B., Di Donato, M., Pezone, A., Di Zazzo, E., Giovannelli, P., Galasso, G., Castoria, G. and Migliaccio, A. 2020. ROS in cancer therapy: the bright side of the moon. *Exp. Mol. Med.* **52**: 192–203.

Pinho, S. S., Carvalho, S., Cabral, J., Reis, C. A. and Gärtner, F. 2012. Canine tumors: a spontaneous animal model of human carcinogenesis. *Transl. Res.* **159**: 165–172.

Plosker, G. L. and Croom, K. F. 2005. Sulfasalazine a review of its use in the management of rheumatoid arthritis. *Drugs*. **65**: 1825–1849.

Pradhan, M., Abeler, V. M., Danielsen, H. E., Sandstad, B., Tropé, C. G., Kristensen, G. B. and Risberg, B. Å. 2012. Prognostic importance of DNA ploidy and DNA index in stage I and II endometrioid adenocarcinoma of the endometrium. *Ann. Oncol.* **23**: 1178–1184.

Prince, M. E., Sivanandan, R., Kaczorowski, A., Wolf, G. T., Kaplan, M. J., Dalerba, P., Weissman, I. L., Clarke, M. F. and Ailles, L. E. 2007. Identification of a subpopulation of

cells with cancer stem cell properties in head and neck squamous cell carcinoma. *Proc. Natl. Acad. Sci.* **104**: 973–978.

Quintana, E., Shackleton, M., Sabel, M. S., Fullen, D. R., Johnson, T. M. and Morrison, S. J. 2008. Efficient tumour formation by single human melanoma cells. *Nature*. **456**: 593–598.

Raybaud, H., Fortin, A., Bairati, I., Morency, R., Monteil, R. A., Nuclear, B. T., Raybaud, H., Fortin, A., Bairati, I., Morency, R., Monteil, R. A. and Bernard, T. 2000. Nuclear DNA content , an adjunct to p53 and Ki-67 as a marker of resistance to radiation therapy in oral cavity and phawngeal squamous cell carcinoma. *Int. J. oral Maxillofac. Surg.* 36–41.

Reczek, C. R. and Chandel, N. S. 2017. The Two Faces of Reactive Oxygen Species in Cancer. *Annu. Rev. Cancer Biol.* **1**: 79–98.

Reynolds, B. A. and Weiss, S. 1992. Generation of neurons and astrocytes from isolated cells of the adult mammalian central nervous system. *Science.* **255**: 1707–1710.

Ribas, V., GarcÃa-Ruiz, C. and FernÃ¡ndez-Checa, J. C. 2014. Glutathione and mitochondria. *Front. Pharmacol.* **5**: 1–19.

Rogez, B., Pascal, Q., Bobillier, A., Machuron, F., Lagadec, C., Tierny, D., Le Bourhis, X. and Chopin, V. 2019. CD44 and CD24 Expression and Prognostic Significance in Canine Mammary Tumors. *Vet. Pathol.* **56**: 377–388.

Roos, W. P., Binder, A. and Bohm, L. 2000. Determination of the initial DNA damage and

residual DNA damage remaining after 12 hours of repair in eleven cell lines at low doses of irradiation. *INT. J. RADIAT. Biol.* **76**: 1493–1500.

Rozemuller, H., Prins, H.-J., Naaijkens, B., Staal, J., Bühring, H.-J. and Martens, A. C. 2010. Prospective isolation of mesenchymal stem cells from multiple mammalian species using cross-reacting anti-human monoclonal antibodies. *Stem Cells Dev.* **19**: 1911–1921.

Rycaj, K. and Tang, D. G. 2014. Cancer stem cells and radioresistance. *Int. J. Radiat. Biol.* **90**: 615–621.

Salerno, M., Avnet, S., Bonuccelli, G., Eramo, A., De Maria, R., Gambarotti, M., Gamberi, G. and Baldini, N. 2013. Sphere-forming cell subsets with cancer stem cell properties in human musculoskeletal sarcomas. *Int. J. Oncol.* **43**: 95–102.

Santos, J. H., Hunakova, L., Chen, Y., Bortner, C. and Van Houten, B. 2003. Cell sorting experiments link persistent mitochondrial DNA damage with loss of mitochondrial membrane potential and apoptotic cell death. *J. Biol. Chem.* **278**: 1728–1734.

Sato, K., Shimokawa, T. and Imai, T. 2019. Difference in acquired radioresistance induction between repeated photon and particle irradiation. *Front. Oncol.* **9**: 1–12.

Schaaf, M. B., Garg, A. D. and Agostinis, P. 2018. Defining the role of the tumor vasculature in antitumor immunity and immunotherapy. *Cell Death Dis.* **9**: 115.

Schmid, I. and Sakamoto, K. M. 2001. Analysis of DNA content and green fluorescent

protein expression. *Curr. Protoc. Cytom.* **16**: 1–10.

Schwartz, J. L., Murnane, J. and Weichselbaum, R. R. 1999. The contribution of DNA ploidy to radiation sensitivity in human tumour cell lines. *Br. J. Cancer*. **79**: 744–747.

Sekhar, K. R., Wang, J., Freeman, M. L. and Kirschner, A. N. 2019. Radiosensitization by enzalutamide for human prostate cancer is mediated through the DNA damage repair pathway. *PLoS One*. **14**: e0214670.

Shaikh, M. V., Kala, M. and Nivsarkar, M. 2016. CD90 a potential cancer stem cell marker and a therapeutic target. *Cancer Biomarkers*. **16**: 301–307.

Shen, Y., Wang, C., Hsieh, Y., Chen, Y. and Wei, Y. 2015. Metabolic reprogramming orchestrates cancer stem cell properties in nasopharyngeal carcinoma. *Cell Cycle*. **14**: 86–98.

Shi, C. J., Gao, J., Wang, M., Wang, X., Tian, R., Zhu, F., Shen, M. and Qin, R. Y. 2011. Cd133+ gallbladder carcinoma cells exhibit self-renewal ability and tumorigenicity. *World J. Gastroenterol*. **17**: 2965–2971.

Shimamura, M., Yamamoto, K., Kurashige, T. and Nagayama, Y. 2018. Intracellular redox status controls spherogenicity, an in vitro cancer stem cell marker, in thyroid cancer cell lines. *Exp. Cell Res.* **370**: 699–707.

Shitara, K., Doi, T., Nagano, O., Imamura, C. K., Ozeki, T., Ishii, Y., Tsuchihashi, K., Takahashi, S., Nakajima, T. E., Hironaka, S., Fukutani, M., Hasegawa, H., Nomura, S., Sato,

A., Einaga, Y., Kuwata, T., Saya, H. and Ohtsu, A. 2017. Dose-escalation study for the targeting of CD44v+ cancer stem cells by sulfasalazine in patients with advanced gastric cancer (EPOC1205). *Gastric Cancer*. **20**: 341–349.

Singh, S. K., Hawkins, C., Clarke, I. D., Squire, J. A., Bayani, J., Hide, T., Henkelman, R. M., Cusimano, M. D. and Dirks, P. B. 2004. Identification of human brain tumour initiating cells. *Nature*. **432**: 396–401.

Snyder, V., Reed-Newman, T. C., Arnold, L., Thomas, S. M. and Anant, S. 2018. Cancer stem cell metabolism and potential therapeutic targets. *Front. Oncol.* **8**: 1–9.

Song, Z., Pearce, M. C., Jiang, Y., Yang, L., Goodall, C., Miranda, C. L., Milovancev, M., Bracha, S., Kolluri, S. K. and Maier, C. S. 2020. Delineation of hypoxia-induced proteome shifts in osteosarcoma cells with different metastatic propensities. *Sci. Rep.* **10**: 727.

Song, Y., Jang, J., Shin, T.-H., Bae, S. M., Kim, J., Kim, K. M., Myung, S.-J., Choi, E. K. and Seo, H. R. 2017. Sulfasalazine attenuates evading anticancer response of CD133-positive hepatocellular carcinoma cells. *J. Exp. Clin. Cancer Res.* **36**: 38.

Stipanuk, M. H., Dominy, J. E., Lee, J. I. and Coloso, R. M. 2006. Mammalian cysteine metabolism: New insights into regulation of cysteine metabolism. *J. Nutr.* **136**: 1652S-1659S.

Stockley, J. H., Evans, K., Matthey, M., Volbracht, K., Agathou, S., Mukanowa, J., Burrone, J. and Káradóttir, R. T. 2017. Surpassing light-induced cell damage in vitro with novel cell culture media. *Sci. Rep.* **7**: 849.

Stoica, G., Lungu, G., Martini-STOICA, H., Waghela, S., Levine, J. and Smith, R. 2009. Identification of cancer stem cells in dog glioblastoma. *Vet. Pathol.* **46**: 391–406.

Sun, L., Moritake, T., Ito, K., Matsumoto, Y., Yasui, H., Nakagawa, H., Hirayama, A., Inanami, O. and Tsuboi, K. 2017. Metabolic analysis of radioresistant medulloblastoma stem-like clones and potential therapeutic targets. *PLoS One*. **12**: e0176162.

Syrios, J., Kechagias, G., Agrogiannis, G., Xynos, I. D., Kavantzas, N., Lazaris, A. C., Amptoulach, S., Mourati, A., Sougioultzis, S., Patsouris, E. S. and Tsavaris, N. 2013. DNA ploidy: a prognostic factor of response to chemotherapy and survival in metastatic gastric adenocarcinoma. *Anticancer Res.* **33**: 1209–14.

Takagi, S., Kitamura, T., Hosaka, Y., Ohsaki, T., Bosnakovski, D., Kadosawa, T., Okumura, M. and Fujinaga, T. 2005. Molecular Cloning of Canine Membrane-Anchored Inhibitor of Matrix Metalloproteinase, RECK. *J. Vet. Med. Sci.* **67**: 385–391.

Tamari, K., Hayashi, K., Ishii, H., Kano, Y., Konno, M., Kawamoto, K., Nishida, N., Koseki, J., Fukusumi, T., Hasegawa, S., Ogawa, H., Hamabe, A., Miyo, M., Noguchi, K., Seo, Y., Doki, Y., Mori, M. and Ogawa, K. 2014. Identification of chemoradiation-resistant osteosarcoma stem cells using an imaging system for proteasome activity. *Int. J. Oncol.* **45**: 2349–2354.

Tanabe, A., Deguchi, T., Sato, T., Nemoto, Y., Maruo, T., Madarame, H., Shida, T., Naya, Y., Ogihara, K. and Sahara, H. 2016. Radioresistance of cancer stem-like cell derived from

canine tumours. *Vet. Comp. Oncol.* **14**: e93–e101.

Tanabe, A., Kimura, K., Tazawa, H., Maruo, T., Taguchi, M. and Sahara, H. 2021. Functional analysis of CD44 variants and xCT in canine tumours. *Vet. Med. Sci.* **7**: 577–585.

Tanaka, K. 2009. The proteasome: Overview of structure and functions. *Proc. Japan Acad. Ser. B*. **85**: 12–36.

Thamm, K., Graupner, S., Werner, C., Huttner, W. B. and Corbeil, D. 2016. Monoclonal antibodies 13A4 and AC133 Do not recognize the canine ortholog of mouse and human stem cell antigen Prominin-1 (CD133). *PLoS One*. **11**: e0164079.

Thanee, M., Padthaisong, S., Suksawat, M., Dokduang, H., Phetcharaburanin, J., Klanrit, P., Titapun, A., Namwat, N., Wangwiwatsin, A., Sa-ngiamwibool, P., Khuntikeo, N., Saya, H. and Loilome, W. 2021. Sulfasalazine modifies metabolic profiles and enhances cisplatin chemosensitivity on cholangiocarcinoma cells in in vitro and in vivo models. *Cancer Metab.* **9**: 11.

Tirino, V., Desiderio, V., D'Aquino, R., De Francesco, F., Pirozzi, G., Galderisi, U., Cavaliere, C., De Rosa, A. and Papaccio, G. 2008. Detection and characterization of CD133+ cancer stem cells in human solid tumours. *PLoS One*. **3**: e3469.

Trachootham, D., Alexandre, J. and Huang, P. 2009. Targeting cancer cells by ROS-mediated mechanisms: a radical therapeutic approach? *Nat. Rev. Drug Discov.* **8**: 579–591.

Tsvetkova, A., Ozerov, I. V., Pustovalova, M., Grekhova, A., Eremin, P., Vorobyeva, N., Eremin, I., Pulin, A., Zorin, V., Kopnin, P., Leonov, S., Zhavoronkov, A., Klokov, D. and Osipov, A. N. 2017. γH2AX, 53BP1 and Rad51 protein foci changes in mesenchymal stem cells during prolonged X-ray irradiation. *Oncotarget*. **8**: 64317–64329.

Tuy, K., Rickenbacker, L. and Hjelmeland, A. B. 2021. Reactive oxygen species produced by altered tumor metabolism impacts cancer stem cell maintenance. *Redox Biol.* **44**: 101953.

Urnauer, S., Müller, A. M., Schug, C., Schmohl, K. A., Tutter, M., Schwenk, N., Rödl, W., Morys, S., Ingrisch, M., Bertram, J., Bartenstein, P., Clevert, D.-A., Wagner, E. and Spitzweg, C. 2017. EGFR-targeted nonviral NIS gene transfer for bioimaging and therapy of disseminated colon cancer metastases. *Oncotarget*. **8**: 92195–92208.

Vlashi, E., Kim, K., Lagadec, C., Donna, L. Della, McDonald, J. T., Eghbali, M., Sayre, J. W., Stefani, E., McBride, W. and Pajonk, F. 2009. In vivo imaging, tracking, and targeting of cancer stem cells. *JNCI J. Natl. Cancer Inst.* **101**: 350–359.

Vlashi, E., Lagadec, C., Chan, M., Frohnen, P., McDonald, A. J. and Pajonk, F. 2013. Targeted elimination of breast cancer cells with low proteasome activity is sufficient for tumor regression. *Breast Cancer Res. Treat.* **141**: 197–203.

Voutsadakis, I. A. 2017. Proteasome expression and activity in cancer and cancer stem cells. *Tumor Biol.* **39**.

Walcher, L., Kistenmacher, A. K., Suo, H., Kitte, R., Dluczek, S., Strauß, A., Blaudszun, A.

R., Yevsa, T., Fricke, S. and Kossatz-Boehlert, U. 2020. Cancer stem cells—origins and biomarkers: Perspectives for targeted personalized therapies. *Front. Immunol.* **11**: 1–33.

Walsh, H. R., Cruickshank, B. M., Brown, J. M. and Marcato, P. 2019. The flick of a switch: Conferring survival advantage to breast cancer stem cells through metabolic plasticity. *Front. Oncol.* **9**: 1–7.

Walter, M. A., Peters, G. E. and Peiper, S. C. 1991. Predicting radioresistance in early glottic squamous cell carcinoma by DNA content. *Ann Otol Rhinol Laryngol*. **100**: 523–526.

Wang, H., Jiang, H., Van De Gucht, M. and De Ridder, M. 2019. Hypoxic radioresistance: Can ROS be the key to overcome it? *Cancers (Basel).* **11**: 112.

Wang, T.-C., Cheng, C.-Y., Yang, W.-H., Chen, W.-C. and Chang, P.-J. 2015. Characterization of highly proliferative secondary tumor clusters along host blood vessels in malignant glioma. *Mol. Med. Rep.* **12**: 6435–6444.

Wang, V. M. Y., Ferreira, R. M. M., Almagro, J., Evan, T., Legrave, N., Zaw Thin, M., Frith, D., Carvalho, J., Barry, D. J., Snijders, A. P., Herbert, E., Nye, E. L., MacRae, J. I. and Behrens, A. 2019. CD9 identifies pancreatic cancer stem cells and modulates glutamine metabolism to fuel tumour growth. *Nat. Cell Biol.* **21**: 1425–1435.

Webster, J. D., Yuzbasiyan-Gurkan, V., Trosko, J. E., Chang, C.-C. and Kiupel, M. 2007. Expression of the Embryonic Transcription Factor Oct4 in Canine Neoplasms: A Potential Marker for Stem Cell Subpopulations in Neoplasia. *Vet. Pathol.* **44**: 893–900.

Weis, S. M. and Cheresh, D. A. 2011. Tumor angiogenesis: molecular pathways and therapeutic targets. *Nat. Med.* **17**: 1359–1370.

Wilson, H., Huelsmeyer, M., Chun, R., Young, K. M., Friedrichs, K. and Argyle, D. J. 2008. Isolation and characterisation of cancer stem cells from canine osteosarcoma. *Vet. J.* **175**: 69–75.

Xiao and Meierhofer 2019. Glutathione metabolism in renal cell carcinoma progression and implications for therapies. *Int. J. Mol. Sci.* **20**: 3672.

Xu, H., Fu, J., Ha, S.-W., Ju, D., Zheng, J., Li, L. and Xie, Y. 2012. The CCAAT box-binding transcription factor NF-Y regulates basal expression of human proteasome genes. *Biochim. Biophys. Acta - Mol. Cell Res.* **1823**: 818–825.

Yamamori, T., Yasui, H., Yamazumi, M., Wada, Y., Nakamura, Y., Nakamura, H. and Inanami, O. 2012. Ionizing radiation induces mitochondrial reactive oxygen species production accompanied by upregulation of mitochondrial electron transport chain function and mitochondrial content under control of the cell cycle checkpoint. *Free Radic. Biol. Med.* **53**: 260–270.

Yamazaki, H., Iwano, T., Otsuka, S., Kagawa, Y., Hoshino, Y., Hosoya, K., Okumura, M. and Takagi, S. 2015. SiRNA knockdown of the DEK nuclear protein mRNA enhances apoptosis and chemosensitivity of canine transitional cell carcinoma cells. *Vet. J.* **204**: 60–65.

Yang, L., Chen, P., Zhang, L., Wang, L., Sun, T., Zhou, L., Li, Z. and Wu, A. 2020. Prognostic value of nucleotyping, DNA ploidy and stroma in high-risk stage II colon cancer. *Br. J. Cancer*. **123**: 973–981.

Ye, P., Mimura, J., Okada, T., Sato, H., Liu, T., Maruyama, A., Ohyama, C. and Itoh, K. 2014. Nrf2- and ATF4-dependent upregulation of xCT modulates the sensitivity of T24 bladder carcinoma cells to proteasome inhibition. *Mol. Cell. Biol.* **34**: 3421–3434.

Yi, H.-G., Jeong, Y. H., Kim, Y., Choi, Y.-J., Moon, H. E., Park, S. H., Kang, K. S., Bae, M., Jang, J., Youn, H., Paek, S. H. and Cho, D.-W. 2019. A bioprinted human-glioblastoma-on-a-chip for the identification of patient-specific responses to chemoradiotherapy. *Nat. Biomed. Eng.* **3**: 509–519.

Yin, S., Li, J., Hu, C., Chen, X., Yao, M., Yan, M., Jiang, G., Ge, C., Xie, H., Wan, D., Yang, S., Zheng, S. and Gu, J. 2007. CD133 positive hepatocellular carcinoma cells possess high capacity for tumorigenicity. *Int. J. Cancer*. **120**: 1444–1450.

Zaidi, M., Fu, F., Cojocari, D., McKee, T. D. and Wouters, B. G. 2019. Quantitative visualization of hypoxia and proliferation gradients within histological tissue sections. *Front. Bioeng. Biotechnol.* **7**: 1–9.

Zhong, Y., Guan, K., Guo, S., Zhou, C., Wang, D., Ma, W., Zhang, Y., Li, C. and Zhang, S. 2010. Spheres derived from the human SK-RC-42 renal cell carcinoma cell line are enriched in cancer stem cells. *Cancer Lett.* **299**: 150–160.

Zhu, X., Chen, H. H., Gao, C. Y., Zhang, X. X., Jiang, J. X., Zhang, Y., Fang, J., Zhao, F. and Chen, Z. G. 2020. Energy metabolism in cancer stem cells. *World J. Stem Cells*. **12**: 448–461.

Abstract of the Dissertation

A study on radio-resistance mechanism of cancer stem-like cells using a property of low proteasome activity in canine tumor cell lines

Cancer stem-like cells (CSCs) form a distinct subpopulation of tumor cells with self-renewal capacity, asymmetric cell division, and tumorigenic potential. In addition to the stem-like properties of CSCs, radio-resistance of CSCs makes it difficult to eradicate tumor cells by radiation therapy as survived CSCs after irradiation cause tumor recurrence. Research for targeting canine CSCs has been tried using several methods such as sphere formation or side population, but there are still problems for identification and isolation of the small population. Recently, visualization of CSCs has been realized in human tumor cells using a property of low proteasome activity in CSCs. However, applicability of the system in canine tumor cells is not clear.

Radio-resistance and survival of tumor cells causing recurrence of tumor are main challenges in veterinary radiation therapy. Among heterogenous tumor cells, particularly, CSCs are the main reason of the radio-resistance of tumors. Therefore, radio-resistance related factors were examined in human tumors including degree of DNA double-strand break after irradiation, DNA contents, mitochondrial respiration, level of reactive species accumulation, glutathione (GSH) synthesis, and so forth. Nevertheless, effective molecular target of CSCs for radiation therapy is still vague, especially, in isolated CSCs using the property of low proteasome activity.

Thus, the present dissertation was planned to evaluate the radiosensitivity and radio-resistance mechanism of canine CSCs for targeting CSCs in radiation therapy. The first objective was to visualize canine CSCs using a property of low proteasome activity. The second objective was to assess radiosensitivity of the visualized CSCs and to find a molecular target for radiosensitization of the visualized CSCs.

The first study imaged canine tumor cells with low proteasome activity using HMPOS and MegTCC. Subsequently, CSC-like properties of the canine tumor cells with low proteasome activity were evaluated, and the visualized cells exhibited asymmetric cell division, up-regulation of CSC markers, and tumorigenic capacity. In the second study, the visualized canine CSCs were employed, and radiosensitivity and radio-resistance mechanism of the canine CSCs were evaluated. Then, radiosensitizing effects of sulfasalazine which inhibits function of xCT and synthesis of GSH were evaluated using the visualized canine CSCs. The visualized canine CSCs exhibited radio-resistance and high GSH contents compared with non-visualized cells. In addition, the visualized cells showed high protein level of xCT. As a result, application of sulfasalazine effectively radio-sensitized the visualized CSCs in canine osteosarcoma cells by reducing GSH contents.

The conclusion of the current dissertation was that canine CSCs were successfully visualized using low proteasome activity, and this visualization system could be a valuable research tool for future CSC research to make CSC-targeting therapeutic approach. Moreover, the radio-resistance and high GSH contents of canine CSCs were revealed owing to high protein level of xCT at low proteasome activity. Also, Sulfasalazine effectively radiosensitized CSCs in canine osteosarcoma cells. These findings suggest the direction of radiation therapy targeting CSCs for successful tumor eradication.

Acknowledgments

The completion of this thesis could not have been possible without the scientific support and participation of many people.

First, I would like to convey my sincere appreciation to my Prof. Masahiro Okumura for allowing me to do research associated with doctoral studies in the Laboratory of Veterinary Surgery, Hokkaido University and for making this work possible with his extensive knowledge, sincerest advice, and patience as well as continuous support in the past few years.

I would like to hearty thank the rest of my co-supervisors: Associate Prof. Kenji Hosoya, Assistant Prof. Takafumi Sunaga, Assistant Prof. Sangho Kim, and Specially Appointed Assistant Prof. Tatsuya Deguchi for their immeasurable supports and scientific advice.

I wish to express my deep acknowledgment to my advisors: Prof. Osamu Inanami, Prof. Takashi Kimura, and Associate Prof. Hironobu Yasui for their brilliant comments, incisive questions which enlighten me to broaden my perspective on the research, and encouragement.

I would like to express my profound gratitude to Associate Prof. Kensuke Takada and Assistant Prof. Keisuke Aoshima for their assistance for the cell sorting and histopathology techniques as well as insightful comments.

I would like to show my deep appreciation to Prof. Minoru Takata and Dr. Yoko Katsuki for allowing my internship in the Radiation Biology Center, Kyoto University and kind teaching of experiment techniques related to radiation biology.

Many thanks to Dr. Yusuke Murase for his persistent help for me to get adjusted to the doctoral course and keep going forward. My sincere thanks also go to all members of my

laboratory, Dr. Suranji Wijekoon, Mijiddorj Tsogbadrakh, Ekkapol Akaraphutiporn, Takachika Sato, Wang Yanlin, Mwale Carol, Ryo Owaki, Akitake Oh, Mika Sumita, and Nanami Maeda for their invaluable supports and wonderful friendship during the study in the Laboratory of Veterinary Surgery.

I would like to offer my special thanks to Prof. Gonhyung Kim, College of Veterinary Medicine, Chungbuk National University for his guidance and continuous mentoring. I could not have imagined standing here without his help.

I extend my sincere condolences to the sacrificed laboratory mice to accomplish this study.

My great acknowledgments to Hokkaido University President's Fellowship for financial contribution during my stay at Hokkaido University.

Lastly, I sincerely thank to my parents, sister, and brother for being supportive and for their encouragement throughout my life. This accomplishment would not have been possible without them.

Hokkaido University, 2022

Dr. Koangyong Sung